

# The Cross-correlation of MgII Absorption and Galaxies in BOSS

Ignasi Pérez-Ràfols,<sup>1,2\*</sup> Jordi Miralda-Escudé,<sup>1,3</sup> Britt Lundgren,<sup>4,5</sup> Jian Ge,<sup>6</sup> Patrick Petitjean,<sup>7</sup> Donald P. Schneider,<sup>8,9</sup> Donald G. York<sup>10</sup> and Benjamin A. Weaver<sup>11</sup>

<sup>1</sup>*Institut de Ciències del Cosmos, Universitat de Barcelona/IEEC, Barcelona E-08028, Catalonia*

<sup>2</sup>*Departament d'Astronomia i Meteorologia, Facultat de Física, Universitat de Barcelona, E-08028 Barcelona, Catalonia*

<sup>3</sup>*Institució Catalana de Recerca i Estudis Avançats, Barcelona, Catalonia*

<sup>4</sup>*Department of Astronomy, University of Wisconsin - Madison, 475 North Charter Street, Madison, WI 53706 USA*

<sup>5</sup>*National Science Foundation Astronomy and Astrophysics Postdoctoral Fellow*

<sup>6</sup>*Department of Astronomy, University of Florida, Bryant Space Science Center, Gainesville, FL 32611-2055, USA*

<sup>7</sup>*Institut d'Astrophysique de Paris, UPMC & CNRS, UMR7095 98bis Boulevard Arago, 75014 - Paris, France*

<sup>8</sup>*Department of Astronomy and Astrophysics, The Pennsylvania State University, University Park, PA 16802*

<sup>9</sup>*Institute for Gravitation and the Cosmos, The Pennsylvania State University, University Park, PA 16802*

<sup>10</sup>*Department of Astronomy and Astrophysics and the Enrico Fermi Institute, University of Chicago, 5640 South Ellis Avenue, Chicago, IL 60637, USA*

<sup>11</sup>*Center for Cosmology and Particle Physics, New York University, New York, NY 10003 USA*

Released 2014 Xxxxx XX

## ABSTRACT

We present a measurement of the cross-correlation of MgII absorption and massive galaxies, using the DR11 main galaxy sample of the Baryon Oscillation Spectroscopic Survey of SDSS-III (CMASS galaxies), and the DR7 quasar spectra of SDSS-II. The cross-correlation is measured by stacking quasar absorption spectra shifted to the redshift of galaxies that are within a certain impact parameter bin of the quasar, after dividing by a quasar continuum model. This results in an average MgII equivalent width as a function of impact parameter from a galaxy, ranging from 50 kpc to more than 10 Mpc in proper units, which includes all MgII absorbers. We show that special care needs to be taken to use an unbiased quasar continuum estimator, to avoid systematic errors in the measurement of the mean stacked MgII equivalent width. The measured cross-correlation follows the expected shape of the galaxy correlation function, although measurement errors are large. We use the cross-correlation amplitude to derive the bias factor of MgII absorbers, finding  $b_{\text{MgII}} = 2.33 \pm 0.19$ , where the error accounts only for the statistical uncertainty in measuring the mean equivalent width. This bias factor is larger than that obtained in previous studies and may be affected by modeling uncertainties that we discuss, but if correct it suggests that MgII absorbers at redshift  $z \simeq 0.5$  are spatially distributed on large scales similarly to the CMASS galaxies in BOSS.

**Key words:** galaxies: haloes, galaxies: formation, quasars: absorption lines, large-scale structure of universe

## 1 INTRODUCTION

The Mg II doublet absorption line, at rest-frame wavelengths  $\lambda = 2796.3543 \text{ \AA}$  and  $2803.5315 \text{ \AA}$ , is an extremely useful tracer of photoionized gas clouds in galactic halos. Several reasons account for this trait: magnesium is among the most abundant of the heavy elements, the oscillator strength of

this Mg II doublet is particularly large, its rest-frame wavelength makes it easily observable from ground-based telescopes at redshifts  $z > 0.3$ , and magnesium is mostly in the form of Mg II in photoionized, self-shielded clouds at the typical pressures of galactic halos. Gas clouds with atomic hydrogen column densities  $N_{\text{HI}} \lesssim 2 \times 10^{17} \text{ cm}^{-2}$  are optically thin to photons above the hydrogen ionization potential of 13.6 eV, as well as to the harder photons that ionize Mg II. Most of the magnesium is therefore ionized more than once

\* email: iprafols@icc.ub.edu

in thin clouds, greatly reducing the Mg II column density. On the other hand, in optically thick clouds, the shielded magnesium ions are mostly recombined to Mg II, but Mg I has an ionization potential of 7.65 eV (below that of hydrogen) and is ionized by photons that penetrate the region of self-shielded hydrogen. Hence, self-shielded clouds in galactic halos should have most of their magnesium as Mg II (e.g., Bergeron & Stasińska 1986). In fact, most strong Mg II systems are also Lyman limit systems, i.e., their HI column densities are high enough to be self-shielding (Rao et al. 2006).

The rest-frame equivalent width distribution of Mg II absorption systems is approximated by an exponential form,  $dN/dz \propto \exp(-W/W^*)$ , with a value  $W^* \simeq 0.6$  at  $z = 0.5$  that increases gradually with redshift, and an excess of systems over this form at  $W < 0.3 \text{ \AA}$  (Nestor et al. 2005; Narayanan et al. 2007, and references therein). Most of the strong systems have a complex velocity structure, with a velocity dispersion of multiple absorbing components that is characteristic of galaxy velocity dispersions, favoring models of a collection of photoionized clouds randomly moving through a galactic halo (Bahcall 1975; Sargent et al. 1979; Churchill et al. 2000), as had already been proposed by Bahcall & Spitzer (1969).

The association of Mg II absorption systems with galactic halos was firmly established with the work of Lanzetta & Bowen (1990), Bergeron & Boissé (1991), and Steidel et al. (1994). The observations of the frequency of occurrence of Mg II absorbers at different impact parameters from luminous galaxies led to a simple model of halos that are close to spherical, in which absorption with rest-frame equivalent width  $W > 0.3 \text{ \AA}$  is nearly always observed within an impact parameter  $r_p \lesssim 50(L_K/L_K^*)^{0.15}$  kpc of a galaxy of K-band luminosity  $L_K$ , and becomes rapidly weaker at larger radii, independently of the type of galaxy being considered (Steidel 1995). Actually, the natural expectation is that there is a smooth profile of declining mean Mg II absorption strength with impact parameter around a galaxy, caused by a decreasing density of clouds with radius in a galactic halo. This is consistent with more recent work, where the mean Mg II equivalent width (which is indicative of the number of intersected individual clumps with saturated absorption) has been shown to steeply decline with the impact parameter  $r_p$  roughly as  $\bar{W} \propto r_p^{-1.5}$  (Chen et al. 2010a), with a characteristic radius at a fixed  $\bar{W}$  that scales proportionally to  $R_{\text{Mg II}} \propto M_*^{0.3}(\text{sSFR})^{0.1}$  (Chen et al. 2010b), where  $M_*$  is the stellar mass in the galaxy and sSFR is the star formation rate per unit of stellar mass. We also note that this describes the mean profile of Mg II absorption around galaxies, and that there are rare cases where Mg II absorption is absent even at very small impact parameter from luminous galaxies (Johnson et al. 2014).

The large extent of the gaseous halos traced by metal absorbers and their nearly ubiquitous presence around all massive galaxies, with only a weak dependence on the specific star formation rate, are observational facts providing support to a scenario in which the Mg II absorbers are a signature of the accretion process of new material onto galaxies. Accreting gas at the temperatures of virialization in galactic halos is thermally unstable and should naturally form photoionized clouds whenever the cooling time of hot halo gas is short compared to the age of the galaxy. This be-

haviour naturally leads to a two-phase model of gaseous galactic halos, where cool clouds can form in approximate pressure equilibrium with a hot medium and are produced in abundance within the cooling radius (Spitzer 1956; Mo & Miralda-Escudé 1996; Maller & Bullock 2004). On the other hand, there is evidence at small radii pointing to the impact of galactic winds on Mg II absorbers: the absorbers are more numerous near the minor axis of their associated galaxies (Bordoloi et al. 2011, 2012; Kacprzak et al. 2011, 2012; Lundgren et al. 2012). The distribution of Mg II absorption systems around galaxies is therefore likely to be sensitive to processes involving both inflow and outflow of material into and from the regions containing the bulk of the stellar mass in galaxies.

The association of Mg II absorbers with galaxies implies a large-scale cross-correlation of these objects. The cross-correlation is in general a result of two effects. First, if every galaxy is surrounded by a gas halo, a Mg II absorber located at an impact parameter  $r_p$  from a galaxy may actually be associated with this galaxy, and be part of the gas halo around it. Second, the Mg II absorber may be associated with a different galaxy that may be a satellite of the first, or with an unrelated galaxy that is spatially correlated with the first, following the usual galaxy autocorrelation. These are usually described as the 1-halo and 2-halo terms, although Mg II systems are considered to be associated to galaxies, rather than dark matter halos. In the limit of impact parameters much smaller than the typical size of a galaxy halo, the first term, determined by the gas halo profile around each galaxy (e.g., Tinker & Chen 2008), dominates, whereas in the limit of large impact parameters, the second term is the important one. The total cross-correlation is in general a combination of the two terms over a wide range of intermediate impact parameters, and it is impossible to cleanly separate the two contributions. But in the large-scale limit, the cross-correlation of Mg II absorbers and galaxies should follow the form of the galaxy correlation function, with an amplitude that is proportional to the product of the two bias factors of the two populations. Hence, measuring the large-scale clustering amplitude helps determine the bias factor, and therefore the halo population that the Mg II absorbing clouds are associated with.

The large-scale Mg II-galaxy cross-correlation was first measured using the photometric catalog of Luminous Red Galaxies in the Sloan Digital Sky Survey (hereafter, SDSS; see York et al. 2000) and the set of individually detected Mg II absorbers in the spectra of SDSS quasars by Bouché et al. (2004), Bouché et al. (2006), Lundgren et al. (2009), Gauthier et al. (2009) and Lundgren et al. (2011). In the absence of precise galaxy redshifts, only the projected cross-correlation function can be measured. The work by Lundgren et al. (2009), based on a set of 2705 Mg II absorbers with rest-frame equivalent width  $W > 0.8 \text{ \AA}$  over the redshift interval  $0.36 < z < 0.8$ , found that the form of the projected cross-correlation is well matched by the Luminous Red Galaxy auto-correlation in the impact parameter range  $0.3 h^{-1} \text{ Mpc} < r_p < 30 h^{-1} \text{ Mpc}$ , and measured the bias factor of these Mg II systems to be  $b_{\text{Mg}} = 1.10 \pm 0.24$ . Gauthier et al. (2009) performed a similar analysis for a sample of 1158 Mg II absorbers with  $W < 1 \text{ \AA}$  over the redshift interval  $0.4 < z < 0.7$  and found the bias factor of these Mg II systems to be  $b_{\text{Mg}} = 1.36 \pm 0.38$ . Both works found

an indication that weak absorbers, with  $W < 1.5 \text{ \AA}$ , cluster more strongly (i.e., they have a larger bias factor) than strong absorbers, and are therefore located in more massive halos on average, although this result was not of high statistical significance. The method used by Bouché et al. (2006), Lundgren et al. (2009) and Gauthier et al. (2009), based on a catalog of identified Mg II systems, requires careful attention to the selection function of *both* galaxies and Mg II systems through an extensive use of simulations, because the number of absorbers will obviously be enhanced in regions of the survey containing more galaxies and more quasar spectra, or where the spectra are of higher signal-to-noise ratio, owing to variable observing conditions and also intrinsic clustering of the quasar sources.

We present a different approach in this paper to measure the cross-correlation of massive galaxies and Mg II absorbers, based on the galaxies with spectroscopically-measured redshifts of the new Baryon Oscillation Spectroscopic Survey (hereafter, BOSS) of the SDSS-III Collaboration (Eisenstein et al. 2011; Dawson et al. 2013). Instead of identifying individual Mg II absorbers, we use a stacking method to measure the average Mg II absorption around a galaxy as a function of the impact parameter and redshift separation. In other words, we measure the redshift-space cross-correlation function of galaxies and Mg II absorption. Our approach is similar to that of Zhu & Ménard (2013b), who have measured the mean Ca II absorption around galaxies, and to Zhu et al. (2013), who have obtained a similar measurement of the large-scale Mg II absorption; we compare their results with ours and discuss the differences near the end of this paper. The data set we use is described in Section 2, and the method is presented in detail in Sections 3 and 4. We present the results in Section 5, which are applied to infer the mean bias factor of Mg II systems in Section 6. Finally we summarize our conclusions in Section 7. Throughout this paper we use the  $\Lambda$ CDM model with  $H_0 = 68 \text{ km s}^{-1} \text{ Mpc}^{-1}$  and  $\Omega_m = 0.3$ .

## 2 DATA SAMPLE

The first step in the analysis is to identify quasar-galaxy pairs in which the quasar sightline passes within a specified bin of projected proper radius, or impact parameter  $r_p$ , from the foreground galaxy. For the background quasar sample we use the quasar catalogue of Schneider et al. (2010) from the 7th Data Release (DR7, Abazajian et al. 2009) of the SDSS-II Collaboration (Gunn et al. 1998; York et al. 2000; Gunn et al. 2006; Eisenstein et al. 2011; Bolton et al. 2012; Smee et al. 2013), with 105,783 spectroscopically confirmed quasars. For the galaxies, the CMASS catalogue (Dawson et al. 2013) of the SDSS-III Collaboration that is prepared for the 11th Data Release (DR11, extension of the SDSS DR9 (Ahn et al. 2012) and the SDSS DR10 (Ahn et al. 2013)) is used, which contains a total of 938,280 galaxies. The DR11 galaxies represent the majority of the final BOSS sample, also covering most of the sky area included in DR7. We note that this galaxy catalogue is the same that was used by Zhu et al. (2013), even though they refer to it as the Luminous Red Galaxy catalogue. We exclude any galaxies at redshift lower than 0.35, corresponding to  $1+z = \lambda_{\text{min}}/\lambda_{\text{MgII}}$ , where we set  $\lambda_{\text{min}} = 3800 \text{ \AA}$  as the shortest wavelength with

sufficient signal-to-noise ratio to provide a useful Mg II absorption signal. This requirement reduces the galaxy sample to 895,472 galaxies. The quasar sample could be increased by including the DR11 sample from BOSS, but most of the new quasars in DR11 are fainter than those in DR7 (having therefore lower S/N) and are at a high redshift, at which the Mg II lines associated with the CMASS galaxies appear superposed with the Ly $\alpha$  forest.

The mean Mg II absorption around galaxies is computed by stacking all the spectra within a certain range of impact parameters from a galaxy. In general, all quasars probing a line-of-sight within a maximum proper impact parameter that was set to  $r_{p,\text{max}} = 12.8 \text{ Mpc}$  are included in the spectral stacking, provided that the following restrictions are met: first, in order to avoid broad absorption line systems associated with quasar outflows, the redshift of the quasar,  $z_q$ , must be larger than that of the galaxy,  $z_{\text{gal}}$ , by a minimum amount, corresponding to a velocity  $v = 0.04c$ ,

$$1 + z_q > R(1 + z_{\text{gal}}) , \quad (1)$$

where  $R = \sqrt{(1+v/c)/(1-v/c)} \simeq 1.041$ . Second, because the presence of the Ly $\alpha$  forest substantially increases the noise in quasar spectra, pairs where the galaxy Mg II line would fall in the Ly $\alpha$  forest region of the quasar are also excluded; in other words, we require

$$(1 + z_{\text{gal}})\lambda_{\text{MgII}} > (1 + z_q)\lambda_{\alpha} , \quad (2)$$

where  $\lambda_{\text{MgII}} = 2798.743 \text{ \AA}$  is the mean wavelength of the Mg II doublet, and the hydrogen Ly $\alpha$  wavelength is  $\lambda_{\alpha} = 1215.67 \text{ \AA}$  at the rest-frame. Note that the quasars that have been reported to have broad absorption lines are also included in the sample. We tested the effect of removing them and we found that the measurements are not significantly changed. We believe that this is because we are only using small windows on the quasar spectra, and therefore the broad absorption line systems are typically not included in the analysis.

The luminosity and redshift distributions of all the DR11 CMASS galaxies meeting these two conditions for at least one quasar that is within an impact parameter  $b_{\text{max}} = 12.8 \text{ Mpc}$ , as computed from the angular separation at the redshift of the galaxy, are shown in figure 1. Note that the density of quasars in DR7 implies that each galaxy has on average  $\sim 3$  quasars within this impact parameter, therefore the majority of galaxies have at least one quasar pair and these distributions are nearly the same as those of the whole DR11 CMASS sample. These distributions represent the characteristics of the galaxies for which we measure the mean Mg II absorption equivalent width as a function of impact parameter in this paper.

## 3 STACKING PROCEDURE

This section describes the method used to measure the average Mg II absorption equivalent width as a function of impact parameter from the CMASS galaxies. In general, the mean transmission fraction  $\bar{F}$  of light from a background quasar due to Mg II absorption line systems can be written as a function of the impact parameter  $r_p$  and velocity

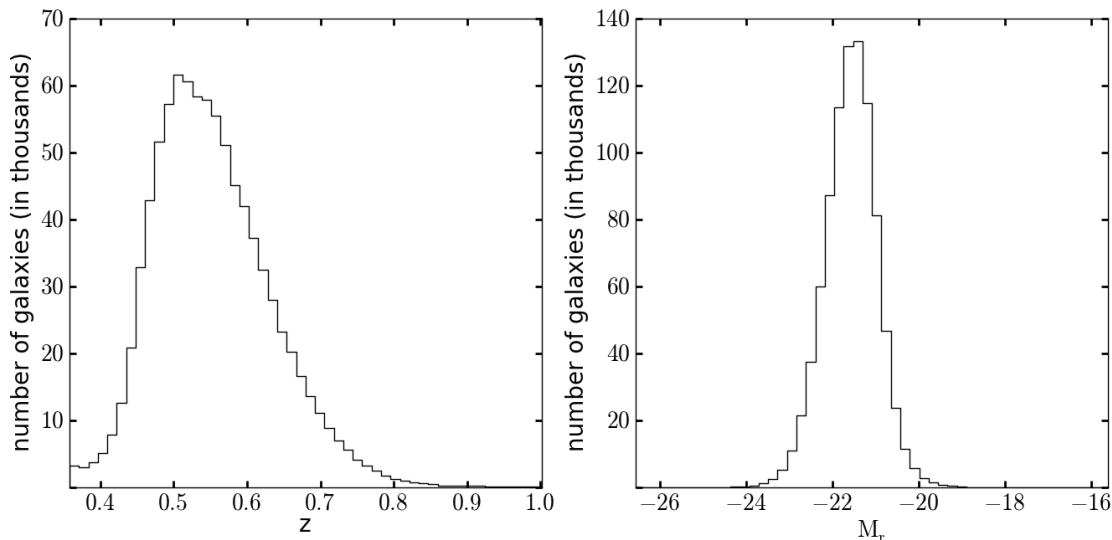


**Figure 1.** Redshift (left panel) and luminosity (right panel) distributions for the selected CMASS galaxies (see text for details) .

separation  $v$  from a galaxy, as

$$\bar{F}(r_p, v) = \exp[-\tau_e(r_p, v)] = \exp[-\tau_{e0}(1 + \delta_{\text{Mg}}(r_p, v))] . \quad (3)$$

Here,  $\tau_e$  is the effective optical depth, and  $\tau_{e0}$  is its average value at any random position, irrespective of the presence of a galaxy. The perturbation  $\delta_{\text{Mg}}$  is the relative increase of the effective optical depth of Mg II absorption associated with the presence of a galaxy at impact parameter  $r_p$  and velocity separation  $v$ . The shape of this perturbation as a function of  $v$ , for a given impact parameter, is rather complicated because it arises from the distribution of relative velocities of a set of doublet lines with different degrees of saturation; besides, the observations are affected by the instrumental resolution and the binning. We will return to these details later.

The mean effective optical depth at a random position can be expressed in terms of the rest-frame equivalent width distribution of Mg II absorbers, as

$$\tau_{e0} = \int_0^\infty dW \frac{\partial^2 \mathcal{N}}{\partial W \partial z} (1+z) \frac{W[1 + \bar{q}(W)]}{\lambda_{\text{MgII}}} , \quad (4)$$

where the equivalent width  $W$  is that of the strongest line of the Mg II doublet at  $\lambda = 2796.35 \text{ \AA}$ , and  $\bar{q}(W)$  is the mean equivalent width ratio of the two doublet lines.

Our aim in this paper is to measure the excess in the effective optical depth,

$$\delta\tau_e(r_p, v) = \tau_e(r_p, v) - \tau_{e0} = \tau_{e0}\delta_{\text{Mg}}(r_p, v) , \quad (5)$$

which is induced by the presence of a galaxy at impact parameter  $r_p$  and velocity separation  $v$ . This quantity is directly related to the cross-correlation of Mg II clouds with CMASS galaxies. We will focus in particular on the projected value of  $\delta\tau_e$ , obtained after integration over velocity, and its relationship to the projected cross-correlation. The method we use to measure this cross-correlation is to average the transmitted fraction over a large number of lines-of-sight within a given range of impact parameter, in order to

reduce the photon noise and the noise arising from quasar continuum variability.

A crucial step to measure the Mg II-galaxy cross-correlation, in the form of  $\delta\tau_e$ , is to estimate the quasar continuum with a method that is, to the best possible degree, free of systematic errors when averaging over a large number of lines-of-sight. In particular, it is important to ensure that the presence of a Mg II line itself, which in most cases may be too weak to be individually detected in the relatively low signal-to-noise ratio SDSS quasar spectra, does not bias the estimate of the continuum. Obviously, if the spectral region where we expect to find the Mg II line associated with a galaxy is used for the continuum determination, the continuum estimate may be systematically biased too low because of the presence of an undetected Mg II line. This systematic bias may be important when stacking large numbers of spectra, even though the Mg II lines causing the bias are not individually detected in any single spectrum.

To illustrate the importance of the quasar continuum determination for the problem of measuring the average Mg II absorption around galaxies at large impact parameters, we explore two different methods and we perform a number of tests for the presence of systematic errors. The first method, designated as *mean subtraction*, is specifically designed for our problem, while the second method, designated as *variable smoothing*, fits a continuum by iteratively smoothing the spectrum with a variable smoothing length to flexibly fit both emission lines and featureless continuum regions. The latter method uses the entire spectrum to determine the continuum, including the region where the associated Mg II line is expected, and is therefore subject to the systematic error described above. We now describe each method in detail. Tests of the methods that show that the mean subtraction method correctly recovers the mean equivalent width and the variable smoothing method is subject to various systematic errors, including the continuum fitting bias mentioned above, are presented in Appendix A.

### 3.1 Method 1: Mean subtraction

The first approach uses the mean spectrum of all quasars as a continuum fit model. Each quasar spectrum is divided by the mean quasar spectrum, and then a linear fit to this ratio is obtained around the spectral region of the expected MgII line for each galaxy-quasar pair, but without using the narrower central interval where the MgII line should be located. This linear fit is used to further improve the continuum estimate, allowing for intrinsic variations of the quasar continua. The results are then stacked for all quasar-galaxy pairs at each interval of impact parameter, after shifting to the redshift of the galaxy in each pair, to obtain the final composite MgII absorption spectrum. We now explain each of these steps in detail.

#### 3.1.1 Generating the mean spectrum

The mean quasar spectrum is generated using the DR7 quasar spectra following a similar approach as the one undertaken by Vanden Berk et al. (2001). The mean spectrum in Vanden Berk et al. (2001) was generated using 1,800 quasars (figure 3 of Vanden Berk et al. 2001), so our mean spectrum is more accurate because of the much larger number of quasars available in DR7. In addition, we normalize the spectra using a spectral window that is particularly suited to obtaining the most accurate continuum model in the region where MgII absorption lines are found. There is therefore a small difference between our mean spectrum and that of Vanden Berk et al. (2001).

The quasar spectra are first shifted to the rest-frame, using the redshifts of Schneider et al. (2010), and rebinned into a common wavelength scale of 1 Å per bin, which is close to the resolution of the observed spectra when shifted to the rest-frame. The values of the flux and the error at each pixel in the new binning are determined by the average values of the flux and error in the original pixels that are projected, partly or fully, to the new pixel, weighted by the fraction of the new bin covered by each original bin. Each quasar spectrum, denoted by an index  $j$ , is normalized with a normalizing factor  $n_j$  equal to the mean flux in the interval 2000 – 2600 Å,

$$n_j = \sum_i f_{ij}/N_j. \quad (6)$$

where  $f_{ij}$  is the measured flux value at pixel  $i$  of spectrum  $j$ , and  $N_j$  is the number of pixels in the rest-frame wavelength interval  $2000 \text{ Å} < \lambda_{ij}(1+z_j) < 2600 \text{ Å}$ . Any quasar spectra that do not cover this entire range of rest-frame wavelength are discarded. The final number of quasar spectra that are averaged in each 1 Å bin is shown in figure 2. The flat top corresponds to the spectral window used to compute the normalizing factor  $n_j$ . Note that the total number of quasar spectra used in this method is 70,650. The maximum number of quasars shown in figure 2, roughly 68,600 quasars, is lower than the total number of spectra used because we remove pixels affected by sky lines. Even though these sky lines are corrected by the BOSS pipeline, the noise in the affected pixels may sometimes not be well characterized, so it is best to remove these pixels. For each sky line, we remove a set of neighboring pixels following the algorithm summarized

in Palanque-Delabrouille et al. (2013) (for a more detailed explanation of the algorithm refer to Lee et al. 2013).

The rest-frame wavelength interval of 2000 – 2600 Å is also used to assign a mean signal-to-noise ratio  $s_j$  to each spectrum, calculated as

$$s_j = \frac{\sum_i f_{ij}/N_j}{(\sum_i e_{ij}^2/N_j)^{1/2}}, \quad (7)$$

where  $e_{ij}$  is the noise of the flux  $f_{ij}$ . The mean, normalized quasar spectrum is then obtained as a weighted average of all the quasar spectra,

$$\bar{f}_i = \frac{\sum_j w_j (f_{ij}/n_j)}{\sum_j w_j}, \quad (8)$$

where the weights  $w_j$  are set equal to

$$w_j = \frac{1}{s_j^{-2} + \sigma_I^2}. \quad (9)$$

The constant  $\sigma_I$  is introduced to avoid the highest signal-to-noise ratio spectra from excessively contributing to the final average, taking into account the presence of intrinsic quasar spectral variability, while reasonably weighting down the more noisy spectra. We fix this constant to  $\sigma_I = 0.05$  (a reasonable estimate for the typical fractional intrinsic variability) throughout this paper. The resulting mean spectrum is shown in figure 3.

#### 3.1.2 Generating the composite MgII absorption spectra

The composite MgII absorption spectra are obtained by stacking the spectra of all the quasars having a galaxy within the corresponding impact parameter bin, after being shifted to the rest-frame of the galaxy in the region around the MgII doublet wavelength. For each quasar-galaxy pair, the quasar spectrum is first rebinned in a velocity variable  $v$ , defined in terms of the wavelength separation from the MgII absorption line in the rest-frame of the galaxy at redshift  $z_{\text{gal}}$ ,

$$v = c \cdot \frac{\lambda - \lambda_0}{\lambda_0}, \quad (10)$$

where  $\lambda_0 = \lambda_{\text{Mg II}}(1+z_{\text{gal}})$ , and  $\lambda_{\text{Mg II}} = 2798.743$ . We use the same linear rebinning method described in Section 3.1.1, with a bin size  $\Delta v = 50 \text{ km s}^{-1}$ . The mean spectrum is also rebinned in the same manner, but using  $\lambda_0 = \lambda_{\text{Mg II}}(1+z_{\text{gal}})/(1+z_q)$ , where  $z_q$  is the quasar redshift, because the mean quasar spectrum is computed in the quasar rest-frame.

The rebinned spectra  $f_{ik}^{(r)}$ , where the  $i$  index now labels the new bins in  $v$ , and the  $k$  index labels each quasar-galaxy pair in a certain impact parameter bin, are then divided by the continuum to obtain a first estimate of the transmission fraction  $F_{ik}^{(0)}$ ,

$$F_{ik}^{(0)} = \frac{f_{ik}^{(r)}/n_{j(k)}}{\bar{f}_i}, \quad (11)$$

where the normalization factor  $n_{j(k)}$  is that of the  $j$  quasar corresponding to each pair  $k$ . The mean quasar spectrum  $\bar{f}$  is understood to be the rebinned one and evaluated at the same bins in  $v$  for each quasar-galaxy pair. Hence, if all quasars had identical intrinsic emission spectra, and in the absence of intervening absorption and observational noise,

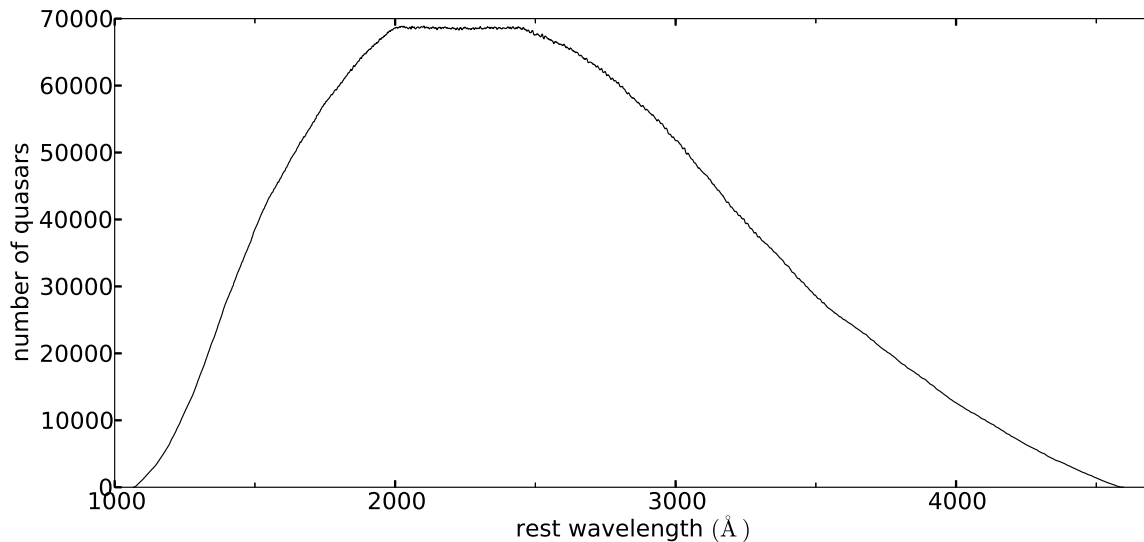


**Figure 2.** Number of quasar spectra contributing to each 1 Å bin of the mean spectrum, as a function of rest-frame wavelength. The flat feature corresponds to the spectral range used to compute the normalizing factor  $n_j$ . Outside this range the number of quasars contributing to the mean quasar spectrum decreases because some of the quasar spectra do not extend to that wavelength.

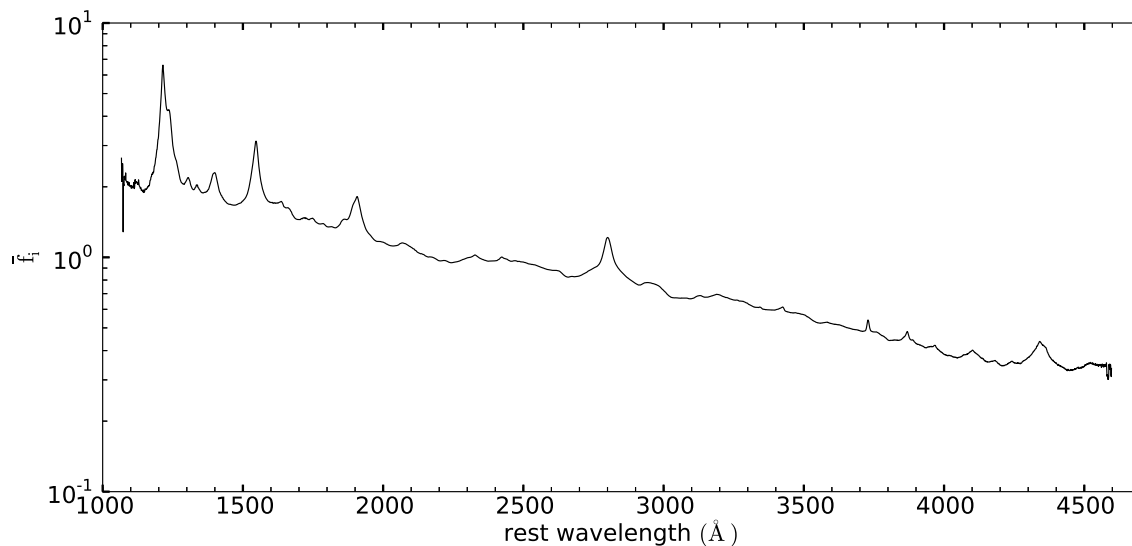


**Figure 3.** Mean spectrum of the weighted-average obtained from the 70,650 DR7 quasars, normalized in the rest-frame wavelength interval from 2000 to 2600 Å. This mean spectrum is used as a continuum model.

this transmission would be equal to unity for all quasars. The errors are normalized in the same way and computed according to  $E_{ij} = e_{ij}/n_j/\bar{f}_i$ .

In order to account for intrinsic variations in the spectra of quasars, we allow for a local smooth gradient in the ratio of each quasar spectrum to the mean spectrum in the region around each expected MgII absorption line. This is modelled by first calculating a weighted average value of  $F_{ik}^{(0)}$  on two intervals in  $v$  on each side of the expected MgII absorption associated with the galaxy, which are far enough from the center so that any associated absorption can be neglected. The intervals used throughout this paper

are  $-5000 \text{ km s}^{-1} < v < -2000 \text{ km s}^{-1}$  and  $2000 \text{ km s}^{-1} < v < 5000 \text{ km s}^{-1}$ , with their weighted averages designated as  $F_k^{(-)}$  and  $F_k^{(+)}$ , respectively. The weights for each bin are set to  $w_{ik} = (\sigma_{n,ik}^2 + \sigma_I^2)^{-1}$ , where  $\sigma_{n,ik} = E_{ik}/F_k^{(+,-)}$  is the inverse signal-to-noise ratio at each pixel (we use the averages  $F_k^{(+)}$  and  $F_k^{(-)}$  for the signal, instead of the values at each pixel  $F_{ik}^{(0)}$ , to avoid biasing the result by systematically giving higher weights to pixels with positive noise). We use, as before,  $\sigma_I = 0.05$ . Weighted averages of the mean velocities  $v_k^{(-)}$  and  $v_k^{(+)}$  are computed in the same manner, which are usually close to the central values of the intervals ( $-3500$  and  $+3500 \text{ km s}^{-1}$ ), but not exactly so. A linear function  $L_{ik}$

matching these two points is then defined,

$$L_{ik} = F_k^{(-)} + (F_k^{(+)} - F_k^{(-)})(v_i - v_k^{(-)}) / (v_k^{(+)} - v_k^{(-)}) . \quad (12)$$

In order to better adjust the quasar continuum in the presence of unrelated random absorption lines or bad pixels, the calculation of the two weighted averages  $F_k^{(-)}$  and  $F_k^{(+)}$  is recomputed after eliminating all outlier pixels in which the normalized flux deviates by more than 3-sigma from the fitted linear function, i.e., pixels where  $\|F_{ik}^{(0)} - L_{ik}\| > 3(\sigma_{n,ik}^2 + \sigma_l^2)^{1/2}$ . If more than 20% of the pixels in any of the two intervals are rejected under this criterion, the quasar spectrum is considered anomalous in the region of the expected MgII line and the quasar-galaxy pair under consideration is rejected and not included in the final processing.

The transmission fraction is then corrected by this linear fit as

$$F_{ik} = F_{ik}^{(0)} + (1 - L_{ik}) . \quad (13)$$

We note here that although it would be in principle more correct to divide by the linear fit, setting  $F_{ik} = F_{ik}^{(0)} / L_{ik}$ , we found that this procedure inevitably introduces a systematic feature in the final stacked spectrum owing to the fact that a Gaussian error in the function  $L$  results in a non-gaussian distribution of the final transmission  $F$  when  $L$  is in the denominator, which is very difficult to correct for. We therefore decided to subtract  $L$  following equation (13).

Finally, we use the same weights as in equation (9) to compute the final composite spectrum and its errors,

$$\bar{F}_i = \frac{\sum_k F_{ik} w_{j(k)}}{\sum_k w_{j(k)}} ; \quad \bar{E}_i^{-2} = \frac{\sum_k E_{ik}^{-2} w_{j(k)}}{\sum_j w_{j(k)}} . \quad (14)$$

The index  $j(k)$  refers to the quasar index  $j$  corresponding to each quasar-galaxy pair labeled by the index  $k$ . In these sums, any pixels over the interval from  $-5000$  to  $+5000 \text{ km s}^{-1}$  with a normalized flux  $F_{ik}$  below  $-2$  or above  $+3$  are eliminated, to exclude bad pixels or values that may have excessive noise. This eliminates only 0.02% of the pixels.

The whole procedure is illustrated in figure 4 with a couple of examples, one with an individually detected Mg II absorption system and one without any individually detected Mg II absorption but with a random metal absorption line. Note that the contribution of these random metal absorption lines is later corrected for (Section 3.3).

### 3.2 Method 2: Variable smoothing

As a second approach to determine the continuum, we use the method described in York et al. (2005), based on an iterative smoothing of the spectrum with a variable smoothing length that is adjusted to decrease in spectral regions of known quasar emission lines. Each quasar spectrum is normalized by dividing both the flux and error by the variable smoothing continuum model,  $c_{ij}$ :

$$F'_{ij} = f_{ij} / c_{ij} ; \quad E'_{ij} = e_{ij} / c_{ij} . \quad (15)$$

In the same way as for the first method, the normalized spectra are rebinned into the variable  $v$  with binwidth of  $50 \text{ km s}^{-1}$ . The final composite spectrum is calculated using the same weights as in equation (9), following equation (14), but using the primed variables  $F'_{ij}$  and  $E'_{ij}$ .

### 3.3 Unbiasing the composite spectra

After the stacking of all the normalized spectra of quasar-galaxy pairs as a function of the velocity variable  $v$  has been completed by using either continuum fitting method, the mean value of the transmission  $\bar{F}_i$  that is obtained far from the expected MgII line (i.e., at large values of  $\|v\|$ ) is close to unity but not exactly so. The main reason for this is the presence of random metal absorption lines (unrelated to the galaxy of the pair) that are detected above a  $3\sigma$  fluctuation and therefore excluded when fitting the continuum. Other reasons may be affecting this mean background of  $\bar{F}_i$  related to systematic effects in the noise distribution and the continuum fitting method. We eliminate this bias by performing the same linear fit to the stacked spectrum as in Section 3.1.2, using again the velocity intervals  $(-5000, -2000)$  and  $(2000, 5000) \text{ km s}^{-1}$  to measure two average values of  $\bar{F}_i$ , and obtaining a linear fit based on two points at the center of these intervals. The final normalized stacked flux is found by dividing by this linear fit.

Our results will actually be shown, for convenience, in terms of the effective excess optical depth, defined according to  $\delta\tau_{e,i} = -\log \bar{F}_i$ , in figures 5 to 7.

### 3.4 Bootstrap errors

The errors computed from the known observational noise in the observed quasar spectra that are stacked are actually a lower limit to the true errors. In reality, the intrinsic variability of real quasar continua and of the associated Mg II and other random metal absorption lines imply the presence of additional errors that are not taken into account and which are correlated among the pixels of the final stacks. We therefore compute bootstrap errors, which are generally used in our analysis and model fits in this paper.

To calculate these bootstrap errors, we use the BOSS plates as the regions of the sky in which the sample is divided. Each quasar is tagged with the plate number at which its best spectrum was observed. For DR7 there are  $N_{\text{plates}} = 1822$  plates Pairs are counted as belonging to the plate that contains the quasar, irrespective of the galaxy position.

Bootstrap errors are computed in the standard way, generating  $N = 1,000$  samples by randomly selecting  $N_{\text{plates}}$  among all the plates with repetition, and then recalculating the composite spectra using both methods. Bootstrap errors are assigned to the final effective optical depth  $\tau_e$ , at each velocity bin and each impact parameter interval from the dispersion found among the 1,000 random samples. These bootstrap errors are computed for both continuum fitting methods.

We note that, specially at large impact parameter, some galaxies will be paired to quasars in different plates. This implies the presence of residual correlations among the bootstrap samples because of the common galaxies in pairs belonging to different plates, but we believe this effect is negligibly small because the most important error correlations should arise from the quasar spectra.

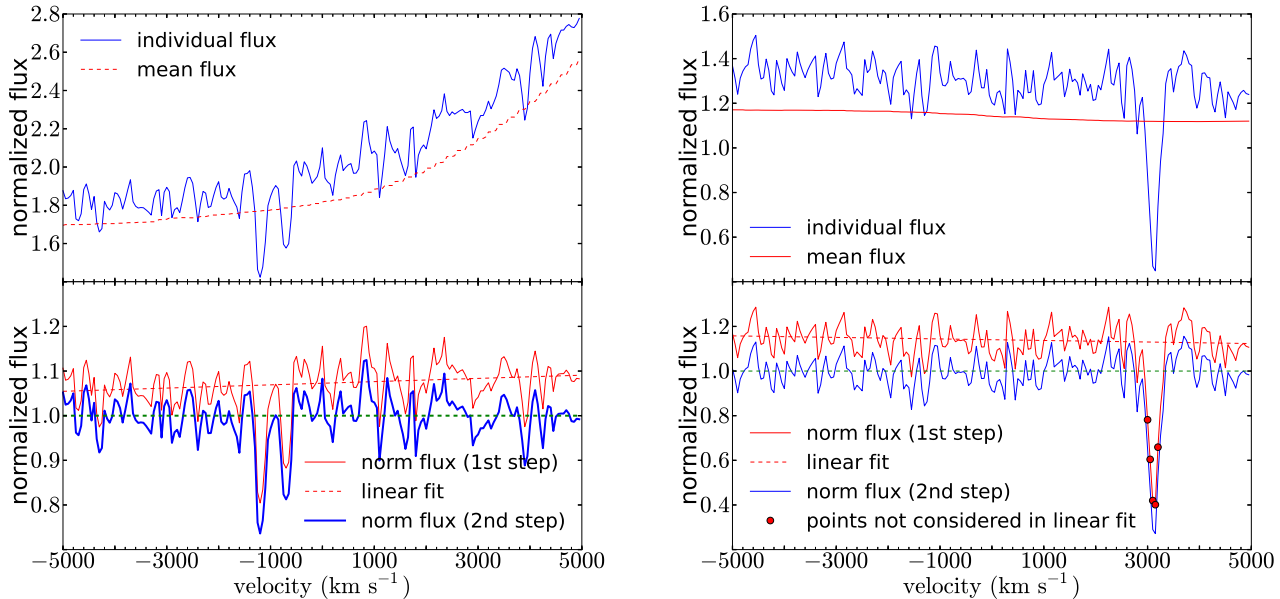


**Figure 4.** Examples illustrating the procedure explained in Section 3.1.2. The left column shows a case with a detected individual Mg II absorption system, and the right column a case with no detectable associated Mg II absorption system, but with an unrelated metal absorption line. The top panels show the normalized flux of the spectral region,  $f_{ik}^{(r)}/n_{j(k)}$  (solid blue line), and the normalized mean spectrum  $\bar{f}_i$  (dashed red line). The bottom panels show the transmission  $F_{ik}^{(0)}$  (thin, solid red line), the computed linear fit  $L_{ik}$  (thin, dashed red line), and the corrected transmission  $F_{ik}$  (thick, solid blue line). In the bottom right panel, the points indicate pixels that are excluded from the linear fit. A horizontal thick dashed green line at a transmission of 1 is included for visual aid.

#### 4 MODEL FOR THE ABSORPTION PROFILE

The usual analysis in the astronomical literature of individual Mg II absorption lines is done by fitting with Voigt profiles, with the equivalent width and the velocity dispersion as free parameters. Whenever the observed absorption profile is not adequately fitted in terms of the two Voigt profiles of the Mg II doublet, one can include the presence of multiple cloud components with blended absorption lines in order to improve the fit. Here, we are analyzing a stack of a large number of Mg II absorption systems that may be mostly undetected individually, but for which we can accurately predict the expected mean position from the redshift of the galaxy near the quasar line of sight. The effective optical depth in the stack,  $\tau_e = -\log(\bar{F})$ , should in this case have a single symmetric component for each line in the doublet, with a profile reflecting the velocity dispersion of Mg II absorbing clouds and galaxies in halos, as well as the large-scale halo correlation in redshift space for large impact parameters. This cross-correlation function can be modeled in terms of the Halo Occupation Distribution formalism (e.g., Gauthier et al. 2008; Zhu & Ménard 2013a), but the density profile of Mg II clouds in halos does not have to follow that of galaxies, and it will generally depend on complex physics of galaxy winds and gas accretion in the circumgalactic medium. For simplicity, we shall assume in this section a model with a Gaussian velocity distribution and a power-law form for the projected correlation function, as an approximation to the generally complex form of the galaxy-absorber cross-correlation function. In the next section, we shall use a more accurate form of the correlation

function obtained from halo simulations to determine the amplitude of our measured cross-correlation.

Our model has four free parameters. The first three are the central effective optical depth  $\tau_0$  of the strongest line in the doublet at a conventional normalization value of the impact parameter  $r_{p0}$  (set here to 1 Mpc), the power-law slope  $\alpha$  of the projected cross-correlation, and the mean equivalent width ratio  $q$  (where  $q = 1/2$  if all the absorption lines were unsaturated, and  $q = 1$  in the saturated case). We consider a variation of the velocity dispersion  $\sigma$  with radius, taking into account that in the limit of large radius, the Hubble expansion should lead to a linear increase of the effective optical depth,  $\delta\tau_e(b, v)$  (as defined in equation 5), is

$$\delta\tau_e(r_p, v) = \frac{\tau_0}{\sqrt{1 + (xHr_p/\sigma_0)^2}} \left( \frac{r_p}{r_{p0}} \right)^{-\alpha} \times \left[ e^{-(v-v_1)^2/2\sigma^2} + q e^{-(v-v_2)^2/2\sigma^2} \right], \quad (16)$$

where

$$\sigma^2 = \sigma_0^2 + (xHr_p)^2. \quad (17)$$

The fourth model parameter is therefore the dimensionless constant  $x$ , which is the scale at which the velocity dispersion starts to increase, compared to  $\sigma_0/H$ , with  $H(z = 0.55) = 91.7$ . In principle, the central velocity dispersion  $\sigma_0$  should also be left as a free parameter, but in this paper we have fixed it to  $250 \text{ km s}^{-1}$ . The reason is that if this condition is relaxed, the obtained fits have a large



degeneracy in  $\sigma_0$  and  $x$  and they are largely dominated by an excess of absorption that is found at the largest impact parameters that we do not fully understand, as we shall see below. The value of  $250 \text{ km s}^{-1}$  allows us to fit well the width of the doublet line at small impact parameter, where it is resolved. Note that the parameter  $q$  is assumed to be independent of impact parameter, even though it may generally depend on it (the mean saturation should decrease with impact parameter if the mean absorber equivalent width also decreases, as suggested by observations; e.g., Gauthier et al. (2009); Chen et al. (2010a)). Note also that the instrumental Point Spread Function (PSF) (Smee et al. 2013) and finite spectral bin size is effectively included in the value of the velocity dispersion in our model. A more detailed modeling of these effects is neglected here for simplicity. The origin of the velocity coordinate  $v$  is chosen by convention as the central position of the Mg II doublet for an unsaturated line ( $q = 0.5$ ) at the redshift of the galaxy. Under this convention,  $v_1 = -256.05 \text{ km s}^{-1}$  and  $v_2 = 513.28 \text{ km s}^{-1}$ .

The fitting is performed by  $\chi^2$  minimization, computed including all the pixels of the stacked spectra in the central interval  $|v| < 2000 \text{ km s}^{-1}$ . Each pixel is weighted according to the bootstrap error measured in that pixel as described in Section 3.4, but without considering the cross-correlations of the errors between pixels. In practice, the bootstrap errorbars in different pixels of the stacked spectra are nearly equal. The spectrum outside the interval  $|v| < 2000 \text{ km s}^{-1}$ , which is used for deriving the continuum fit in Method 1, is not considered here for the fit. We note also that for a real Gaussian profile for each component of the Mg II doublet, the continuum fitting of Method 1 implies that we formally need to subtract a small constant from the double Gaussian in equation (16), equal to the integrated value of the model absorption over the interval  $v \in (2000, 5000) \text{ km s}^{-1}$  used for determining the continuum, but we neglect this effect here.

We use a Monte Carlo Markov Chain method to perform the  $\chi^2$  minimization to the five-parameter model fit. The errors of the parameters are also obtained by repeating the model fit with bootstrap realizations. The average integrated equivalent width as a function of impact parameter can be obtained directly by integrating the effective optical depth over the interval used to fit the model,

$$W_e(r_p) = \frac{\lambda_{\text{Mg II}}}{c} \int_{-2000 \text{ km s}^{-1}}^{2000 \text{ km s}^{-1}} \delta\tau_e(r_p, v) dv. \quad (18)$$

The fitted model also predicts a mean equivalent width,

$$\begin{aligned} W_e(r_p) &= \frac{\lambda_{\text{Mg II}}}{c} \sqrt{2\pi} \tau_0 \sigma_0 (1+q) \left( \frac{r_p}{r_{p0}} \right)^{-\alpha} = \\ &= W_{e0} \left( \frac{r_p}{r_{p0}} \right)^{-\alpha}, \end{aligned} \quad (19)$$

although this value is for the absorption over the whole velocity range, not restricted to the interval  $-2000 \text{ km s}^{-1} < v < 2000 \text{ km s}^{-1}$ .

## 5 RESULTS

The results of the stacked absorption profiles are obtained for a total of 17 impact parameter intervals, measured in

	mean subtraction	variable smoothing
$\tau_0$	$0.0060 \pm 0.0001$	$0.0034 \pm 0.0001$
$\alpha$	$0.70 \pm 0.01$	$0.88 \pm 0.01$
$\sigma_0 [\text{km s}^{-1}]$	250	250
$x$	$1.35 \pm 0.06$	$0.46 \pm 0.08$
$q$	$0.65 \pm 0.03$	$0.66 \pm 0.03$
$W_{e0} [\text{km s}^{-1}]$	$6.27 \pm 0.10$	$3.58 \pm 0.08$

**Table 1.** Best-fit values for the fitted parameters of the model described in Section 4 and shown as the lines in Figure 9. *First column:* Results using the mean subtraction method (see Section 3.1). *Second column:* Results using the variable smoothing method (see Section 3.2). Four independent parameters are fitted, and  $W_{e0}$  is related to the other parameters according to equation (19). As explained in section 4,  $\sigma_0$  is fixed at  $250 \text{ km s}^{-1}$ . Errors are computed from repeating the fits on bootstrap realizations of the stacked profiles.

proper units at the redshift of the galaxy. The first interval is for  $r_p < 50 \text{ kpc}$ , and the other 16 intervals are  $2^{(i-1)/2} < (r_p/50 \text{ kpc}) < 2^{i/2}$ , for  $i = 1$  to 16, up to a maximum impact parameter of 12.8 Mpc. The stacked profiles are shown as the effective optical depth,  $\tau_e = -\log(\bar{F})$ , in figures 5, 6 and 7. Results are presented for our two continuum fitting methods, the mean subtraction method (thick, solid blue line) and the variable smoothing method (thin, solid red line). The errorbars plotted on the left side are the rms value of the bootstrap error of  $\tau_e$  in one pixel, which has little variation among different pixels in each stacked spectrum. The results of the fitted model parameters and their bootstrap errors computed by repeating the fit for bootstrap realizations of the stacked profiles, are given in table 1 (the cross-correlations of the parameter errors are omitted).

The stacks in figures 5, 6 and 7 show the mean absorption profile of the Mg II doublet line, clearly seen at the expected positions at small impact parameters. The amplitude of the random pixel-to-pixel variations outside of the central absorption feature is generally consistent with the computed bootstrap errorbars. The expected doublet feature of the Mg II line is generally resolved at  $r_p \lesssim 200 \text{ kpc}$ , and is smoothed out at larger impact parameter by the velocity dispersion of the absorbers, which should increase linearly with  $r_p$  in the limit of large radius because of Hubble expansion. The fact that our parameter  $x$  is close to unity supports this interpretation, although we note that the precise expected theoretical value of  $x$  in the linear regime is not one because of redshift distortions. We do not analyze this issue further in this paper because the maximum impact parameter that we analyze is not yet in the linear regime, and a more detailed model would be necessary for the velocity distribution of absorbers as a function of impact parameter. We mention here that we initially considered a simpler model with  $x = 0$  and  $\sigma_0$  as free parameter, but this choice gave a substantially worse fit and resulted in a high value of the velocity dispersion because of its increase with radius. As mentioned previously, fits leaving both  $\sigma_0$  and  $x_0$  as free parameters lead to a substantial degeneracy and to solutions with very large values of  $\sigma_0$ , driven by the excess of absorption that is seen in the last  $r_p$  bin for the mean subtraction method. We have not found an explanation for this excess in the last bin, which is only marginally consistent (at the  $\sim 3 - \sigma$  level, as shown below in figure 8) with our fit. A value  $q \simeq 0.65$  is obtained for the line ratio of the

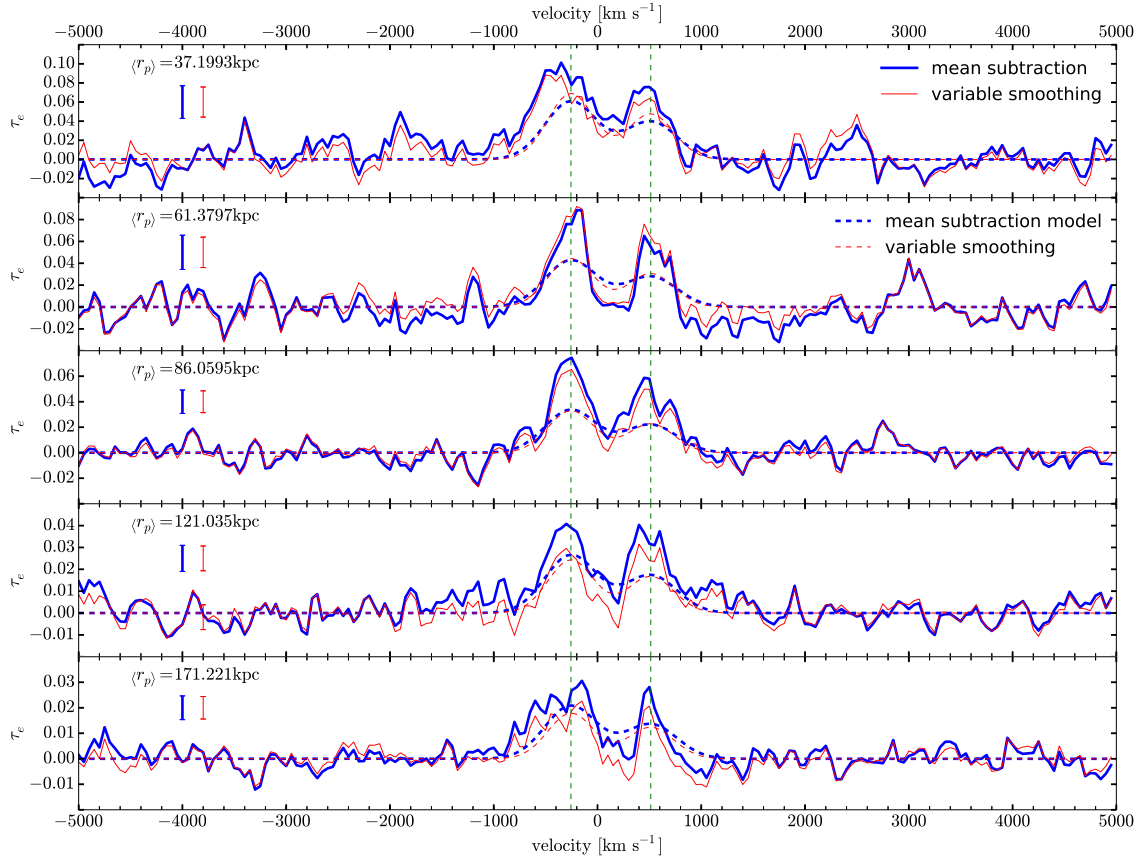


**Figure 5.** From top to bottom, composite spectra for increasing impact parameter intervals (in proper kpc). The effective optical depth is shown against velocity for the mean subtraction method (thick, solid blue line) and the variable smoothing method (thin, solid red line). The rms value of the bootstrap error in individual pixels is shown by the errorbars on the left. The thick, dashed blue line and the thin, dashed red line are the best fit model (equation 16) for the mean subtraction and variable smoothing methods respectively. A single set of parameters are fitted to all the 17 regions. Figures 6 and 7 show the spectra for the remaining impact parameter intervals. The stacks show a mean absorption profile for the presence of the Mg II doublet line at the expected position. For visual guidance, vertical, dashed green lines mark the predicted position of the Mg II doublet.

Mg II doublet, consistent with a mixture of saturated and unsaturated lines. It has been previously reported that the mean equivalent width of the Mg II lines decreases with impact parameter (Gauthier et al. 2009, and references therein). This result may imply that absorbers are less saturated at larger impact parameters, and should therefore have a decreasing value of  $q$ , although this interpretation depends on whether the internal velocity dispersion of the absorbing clouds varies with impact parameter (note that this internal velocity dispersion is much smaller than the velocity dispersion of absorbing components around their host galaxies). Our model assumes a constant value of  $q$  for simplicity.

The mean equivalent widths obtained with our two methods, by directly integrating the effective optical depth in the stacked spectra as in equation (18), are shown in figure 8 as blue triangles for the mean subtraction method, and red squares for the variable smoothing method. These values and their bootstrap errors are also given in table 2, together with the number of galaxy-quasar pairs that contribute to the stacked spectrum at each impact parameter bin. Note

that this mean equivalent width is for the sum of the two lines in the Mg II doublet. There is a systematic difference in the mean equivalent width obtained with the two methods; the variable smoothing method yields a systematically smaller equivalent width compared to the mean subtraction method, and the discrepancy increases with impact parameter, reaching more than a factor 2 at  $r_p = 10$  Mpc. As mentioned previously in Section 3, the reason for this difference is that the spectral region where Mg II absorption is expected is used to determine the continuum in the variable smoothing method. The presence of weak lines that remain undetected in individual spectra causes the continuum to be underestimated in a way that depends on the signal-to-noise ratio and the equivalent width of the undetected line in a complex manner. This systematic underestimate of the continuum causes the underestimate of the mean equivalent width. Appendix A presents quantitative tests demonstrating the presence of this systematic error of the variable smoothing method, and shows also that the result obtained with the mean subtraction method, which does not use the

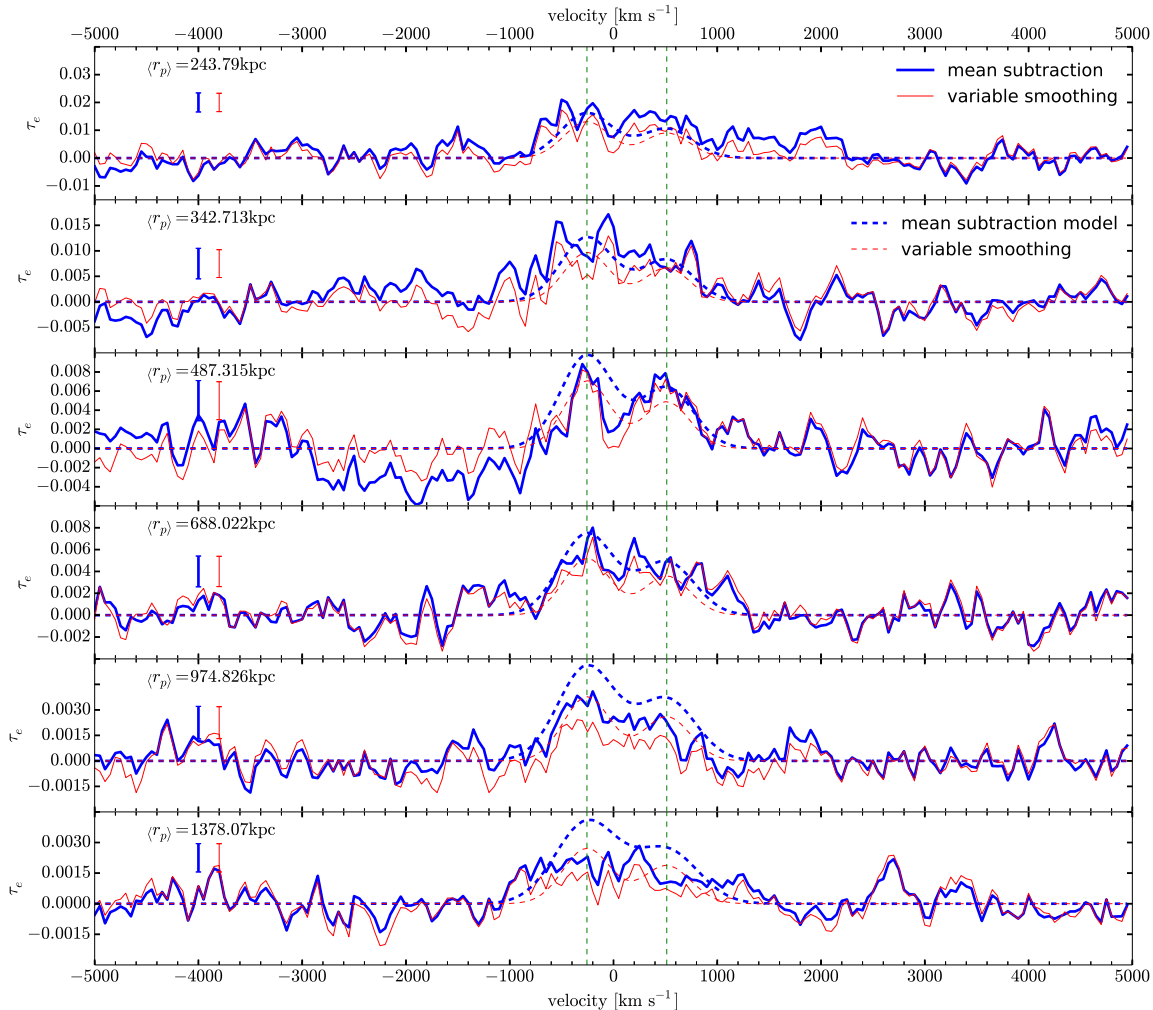


Figure 6. Continuation of figure 5.

stacked spectrum in the region of the Mg II absorption to determine the continuum, is free of any similar systematic effect to the extent that we are able to discern.

The green circles with errorbars in figure 8 show the results of Zhu et al. (2013), who have used a sample of galaxies and quasar spectra similar to ours to infer the same mean equivalent width as a function of impact parameter. Their result is systematically below ours, roughly by a factor  $\sim 2$  at all impact parameters, and is lower even compared to our variable smoothing method. We believe the reason is again due to the systematic underestimate of the continuum. The continuum fitting method used by Zhu et al. (2013) also uses the observed spectra in the region where Mg II absorption is expected in a rather complex way that is described in Zhu & Ménard (2013b), and the systematic error that this induces is difficult to predict but may in principle explain why it produces a systematically low estimate of the equivalent width. Note that in principle this underestimation will only affect the individually undetected systems. Individually

undetected systems cannot be distinguished from the noise and will thus be fitted away by the continuum fitter. Individually detected systems will, in principle, not suffer from this effect. The errorbars of Zhu et al. (2013) are also smaller than ours, since their continuum fitting can better remove any features of the quasar spectrum that are superposed with the Mg II absorption lines, at the cost of introducing a systematic bias in the continuum estimate.

## 6 DISCUSSION

### 6.1 Relation of the mean equivalent width to the bias factor of Mg II absorption systems

Our measurement of the cross-correlation of Mg II absorption systems and galaxies in the CMASS catalog of BOSS clearly reflects properties of the spatial distribution of these two objects. In the limit of large scales, when the fluctuations are in the linear regime, any population of objects

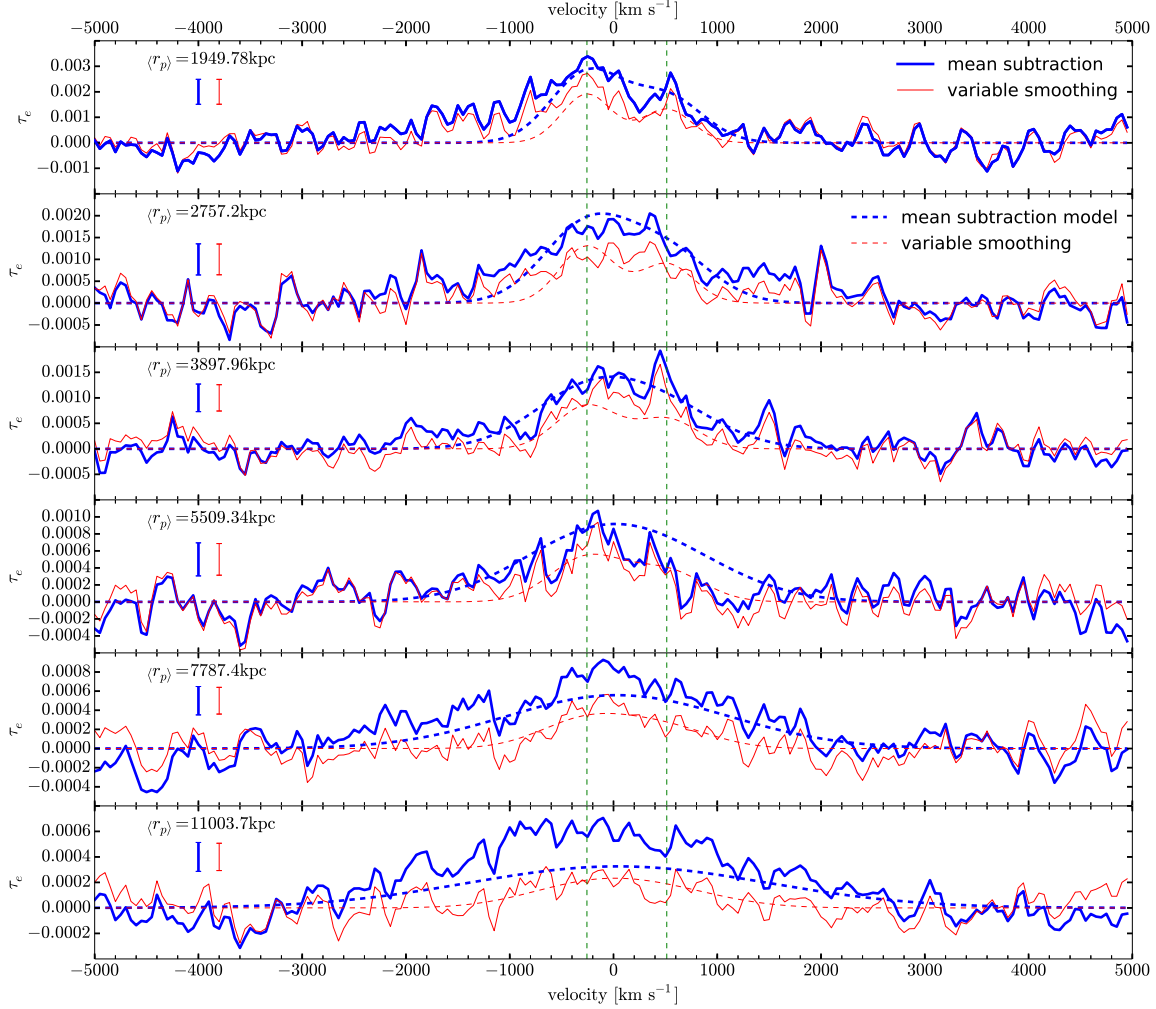


**Figure 7.** Continuation of figure 5.

that traces the large-scale mass perturbations is characterized by its bias factor and the autocorrelation in real space is equal to the correlation function of the mass times the square of the bias factor, with redshift distortions added in redshift space (Kaiser 1987; Cole & Kaiser 1989). The cross-correlation of two classes of objects is, in the same large-scale limit, equal to the mass correlation function times the product of the two bias factors. On small, non-linear scales, the correlations are more complex and they depend on other physics that determine the distribution of galaxies and Mg II absorbers in relation to dark matter halos.

Our stacked spectra measure the mean excess of the effective optical depth as a function of impact parameter  $r_p$  and velocity separation  $v$  from a galaxy. This quantity is related to the mean Mg II absorption perturbation,  $\delta_{\text{Mg}}(r_p, v)$ , as

$$\tau_e(r_p, v) = \tau_{e0} (1 + \delta_{\text{Mg}}(r_p, v)) \quad (20)$$

where  $\tau_{e0}$  is the mean Mg II effective optical depth, de-

finied in equation 4. This perturbation is equal to the cross-correlation function of Mg II absorbers and galaxies, convolved with the mean doublet absorption profile of a Mg II system, and is the function that is measured in our stacking results in figures 5 to 6. In this work, our interest is focused on the projected correlation function, related to the integrated absorption  $W_e(r_p)$  in equation (18). The projected cross-correlation is not affected by redshift distortions and by the complications arising from the convolution with the mean doublet line profile and the spectrograph resolution.

Here, we shall make two approximations to physically interpret our measurement of  $W_e(r_p)$ : first, we neglect the effect of the finite integrating range  $\pm 2000 \text{ km s}^{-1}$  that we have used, ignoring the difference from the true projected correlation that is obtained by integrating to infinity. This approximation is likely not very good for the largest impact parameters we use; we discuss this further below. Second, we assume that the cross-correlation of Mg II systems and CMASS galaxies is the same as the auto-correlation of

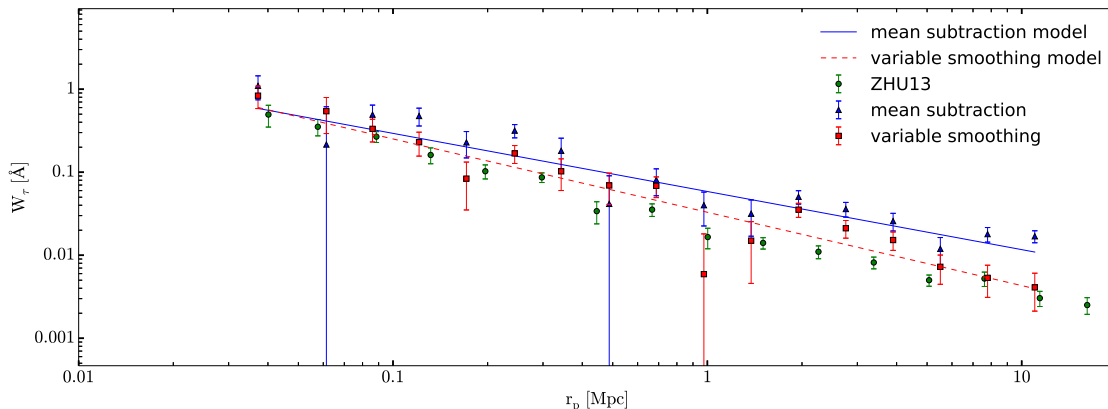


**Figure 8.** Measured rest-frame mean equivalent width  $W_e$  of the MgII doublet, versus proper impact parameter. Blue triangles are obtained from the mean subtraction continuum method, and red squares use the variable smoothing method. Errorbars have been obtained by the bootstrap method. Lines are the best-fit power-law model to the data for both methods. Green circles are the results of Zhu et al. (2013). Note that the results for the mean subtraction method are systematically higher than the rest. This is explored in further detail in the appendix A.

$r_p$ [kpc]	mean subtraction		variable smoothing		$N_{\text{pairs}}$
	$\langle W \rangle$ [Å]	$\sigma(\langle W \rangle)$ [Å]	$\langle W \rangle$ [Å]	$\sigma(\langle W \rangle)$ [Å]	
(0, 50]	1.10	0.35	0.84	0.25	76
(50, 70.71]	0.22	0.40	0.54	0.25	94
(70.71, 100]	0.49	0.15	0.33	0.10	204
(100, 141.42]	0.48	0.12	0.230	0.074	423
(141.42, 200]	0.229	0.080	0.084	0.049	758
(200, 282.84]	0.317	0.058	0.168	0.041	1396
(282.84, 400]	0.181	0.076	0.102	0.042	2621
(400, 565.69]	0.042	0.049	0.069	0.028	4904
(565.69, 800]	0.081	0.029	0.069	0.019	9576
(800, 1131.37]	0.040	0.018	0.006	0.012	19166
(1131.37, 1600]	0.032	0.015	0.015	0.010	38922
(1600, 2262.74]	0.0506	0.0093	0.0354	0.0068	75567
(2262.74, 3200]	0.0360	0.0072	0.0211	0.0051	148769
(3200, 4525.48]	0.0258	0.0062	0.0152	0.0038	290340
(4525.48, 6400]	0.0119	0.0044	0.0073	0.0028	559840
(6400, 9050.97]	0.0180	0.0036	0.0053	0.0022	1062482
(9050.97, 12800]	0.0169	0.0028	0.0041	0.0020	1961450

**Table 2.** Results on the mean equivalent width and errors shown in figure 8, presented here as a table. From left to right, impact parameter interval, mean rest-frame MgII equivalent width and its bootstrap error for the mean subtraction and variable smoothing methods, and number of QSO-galaxy pairs used in the interval. The mean rest-frame equivalent widths are the sum of both lines in the doublet.

CMASS galaxies times the ratio of bias factors  $b_{\text{Mg}}/b_g$  of the two types of objects. In other words, we assume the linear relation can be extended into the non-linear regime as far as the ratio of the cross-correlation to the auto-correlation is concerned.

This second assumption can be justified from observations of the correlations of galaxies of different luminosity. Zehavi et al. (2011) measured the projected correlation of galaxies in the DR7 catalogue in different luminosity ranges, and, to a good approximation, in the impact parameter range of our interest, the result is a fixed shape times the variable bias factor, as seen for example in their figure 6. The shape of the galaxy correlation can be interpreted as arising from the correlation among virialized halos and the distri-

bution of galaxies within each halo (e.g. Zheng et al. 2005). This shape does vary slightly with luminosity, but the most important variation is the normalization determined by the bias factor. There is a greater variation of the shape of the projected correlation with galaxy color (see figure 21 in Zehavi et al. 2011). In addition, the projected cross-correlation of galaxies of different color is not exactly equal to the geometric mean of the projected auto-correlations of the two types of galaxies (see their figure 15). Our assumption can only be considered as a first approximation that will need to be tested in the future, but it allows us to obtain a bias factor for MgII absorption systems assuming that they behave in a similar way as galaxies in the CMASS catalog.

These assumptions lead to the relation

$$W_e(r_p) = \frac{\tau_{e0} \lambda_{\text{Mg II}}}{c} \int dv \delta_{\text{Mg}}(r_p, v) = \frac{\lambda_{\text{Mg II}}}{c} \frac{\tau_{e0} H(z)}{1+z} \frac{b_{\text{Mg}}}{b_g} w_{\text{gg}}(r_p), \quad (21)$$

where  $w_{\text{gg}}(r_p)$  is the projected galaxy correlation function,  $b_g$  is the galaxy bias factor and  $b_{\text{Mg}}$  is the mean bias factor of Mg II absorption systems, weighted in proportion to their equivalent width. We have used  $dv = H(z)/(1+z) dx$ , where  $dx$  is the comoving space coordinate that is integrated to obtain the projected galaxy correlation function, and  $z$  is the mean redshift of the galaxies and associated Mg II absorption systems. This relation allows us to infer the bias factor of Mg II systems empirically, using only the directly measured projected galaxy correlation. Its validity is strictly valid in the limit of large scales, but, as we shall see below, the ratio  $W_e(r_p)/w_{\text{gg}}(r_p)$  is roughly constant, making our assumption plausible as a first approximation.

## 6.2 Mean absorption from Mg II systems

The value of  $\tau_{e0}$ , representing the average absorption from the population of Mg II absorbers, must be independently known before we can use the measured mean excess of Mg II absorption around galaxies to infer the bias factor of Mg II systems with equation (21). This parameter can be estimated from equation (4) using models of the equivalent width distribution that fit the observational data.

We use the double exponential model of Nestor et al. (2005),

$$\frac{\partial^2 \mathcal{N}}{\partial W \partial z} = \frac{N_{\text{wk}}^*}{W_{\text{wk}}^*} \exp^{-W/W_{\text{wk}}^*} + \frac{N_{\text{str}}^*}{W_{\text{str}}^*} \exp^{-W/W_{\text{str}}^*}, \quad (22)$$

where  $N_{\text{str}}^*$  and  $N_{\text{wk}}^*$  are the number of absorbers per unit of redshift in the strong and weak population, and  $W_{\text{str}}^*$  and  $W_{\text{wk}}^*$  are the characteristic rest-frame equivalent widths of the two exponential distributions. This model was fitted by Nestor et al. (2005) to their data, using mocks to correct for incompleteness at low equivalent widths. More recently, a compilation of high-resolution data was shown by Bernet et al. (2010) in their figure 5, reaching down to lower equivalent widths. We include these observational results in figure 9, overplotting the fit that was obtained by Nestor et al. (2005), which has the following parameters:  $N_{\text{wk}}^* = 1.71 \pm 0.02$ ,  $W_{\text{wk}}^* = 0.072 \pm 0.001 \text{ \AA}$ ,  $N_{\text{str}}^* = 0.932 \pm 0.011$  and  $W_{\text{str}}^* = 0.771 \pm 0.014 \text{ \AA}$ . The observations are well reproduced by this fit, which we therefore use to compute  $\tau_{e0}$ .

Unfortunately, the sample of absorbers of Nestor et al. (2005) is somewhat heterogeneous, and the main uncertainty we encounter in using it to compute  $\tau_{e0}$  is due to the redshift evolution. A fit to this evolution was determined by Nestor et al. (2005), where the parameters of the exponential model vary as  $W^* \propto (1+z)^{0.634 \pm 0.097}$  and  $N^* \propto (1+z)^{0.226 \pm 0.170}$ , both for the weak and strong populations. We infer from their model fits and the mean value of  $N^*$  that the mean redshift of their sample is  $z \simeq 1.1$  and we use these relations to convert the product  $N^* W^*$  to the mean redshift of the CMASS galaxy catalog,  $z \simeq 0.55$ . We find  $N_{\text{str}}^* W_{\text{str}}^* = 0.55 \text{ \AA}$  and  $N_{\text{wk}}^* W_{\text{wk}}^* = 0.095 \text{ \AA}$ , with an error that is close to 10%,

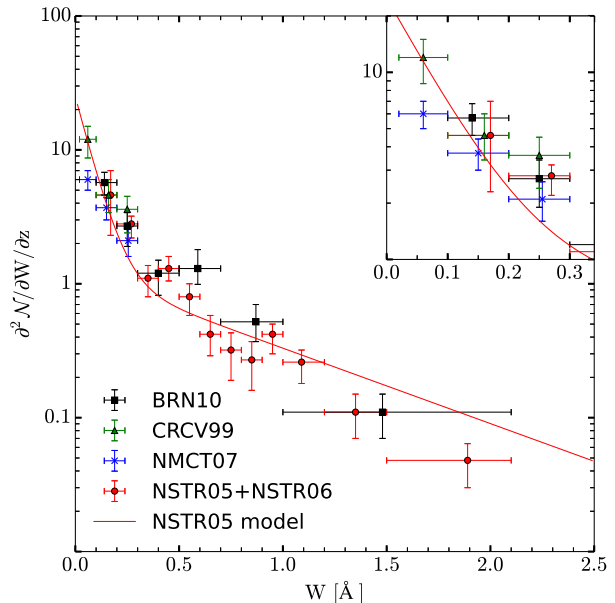


**Figure 9.** Rest-frame equivalent width distribution of Mg II absorption systems. Data points are from Bernet et al. (2010) (black squares), Churchill et al. (1999) (green triangles), Narayanan et al. (2007) (blue crosses) and Nestor et al. (2005, 2006) (red circles). The overlotted solid line is the double exponential fit of Nestor et al. (2005) (see text). Top right panel is a zoomed view of the weakest absorption systems.

although it is poorly defined because the errors in the redshift evolution of  $N_{\text{str,wk}}^*$  and  $W_{\text{str,wk}}^*$  should be correlated, and this information (and the exact redshift distribution of the absorbers) was not provided in Nestor et al. (2005).

From equation 4, we derive the value of  $\tau_{e0}$  in the double exponential model of equation 22,

$$\tau_{e0} = \frac{1+z}{\lambda_{\text{Mg II}}} (1+\bar{q}) (N_{\text{wk}}^* W_{\text{wk}}^* + N_{\text{str}}^* W_{\text{str}}^*). \quad (23)$$

which yields a value  $\tau_{e0}(z = 0.55) = 5.0 \times 10^{-4}$ , with an error of about 10% but which is subject to uncertainties owing to the redshift evolution, the accuracy of the fit to the equivalent width distribution, and the value of  $\bar{q}$ . Our results will be given in terms of  $\tau_{e0}$  without including its error, with the understanding that this quantity will need to be better determined in the future from studies of the field population of Mg II absorbers.

## 6.3 Derivation of the bias factor of Mg II systems

We now use equation 21 to infer the bias factor of the Mg II systems, as

$$b_{\text{Mg}} = b_g \frac{c W_e(r_p)(1+z)}{\tau_{e0} \lambda_{\text{Mg II}} w_{\text{gg}}(r_p) H(z)}. \quad (24)$$

Note that the factor  $(1+z)/H(z)$  appears because of our convention that the effective equivalent width  $W_e$  is measured in  $\text{\AA}$ , whereas  $w_{\text{gg}}$  is assumed to have been transformed to comoving length units. Instead of fitting our Mg II-galaxy cross-correlation measurement with a power-law dependence

with impact parameter (as in equation 16), we can directly fit the functional form that is determined from the observed projected galaxy correlation function, assuming that the shape is the same. To do this, we use the projected galaxy autocorrelation function obtained in Nuza et al. (2013) from the BOSS DR9 catalog of CMASS galaxies, and their prediction for the galaxy correlation function based on assigning galaxies to halos and subhalos in their MultiDark simulation. The measurements of Nuza et al. (2013) are represented as black triangles with errorbars in figure 10, and their model is shown as the thick black line (given in their figure 6 and table B1; note that we have corrected for the different cosmological model they use, with a present matter density  $\Omega_m = 0.27$  instead of our value  $\Omega_m = 0.3$ ). Blue triangles, red squares and green circles are the mean equivalent width  $W_e(r_p)$  times the factor  $(1+z)/H(z)/\tau_{e0}$  (equal to the cross-correlation of Mg II systems and CMASS galaxies), times  $r_p(1+z)$  for the mean subtraction method, the variable smoothing method and measurements from Zhu et al. (2013) respectively.

The galaxy bias factor in the model of Nuza et al. (2013) shown as the dashed black line is  $b_g = 2.00 \pm 0.07$ . Note that this value is lower than that obtained by Guo et al. (2013),  $b_g = 2.16 \pm 0.01$ , for the average CMASS galaxy. Using the value given by Guo et al. (2013) would lead to a larger measured value of the bias factor of the Mg II systems. As explained in Guo et al. (2013), the value of the galaxy bias increases with luminosity and redshift, and it can also depend on the range of scales used to fit its value. Here we use the galaxy bias value and the projected galaxy autocorrelation function of Nuza et al. (2013), but the discrepancy with the higher value obtained by Guo et al. (2013) needs to be resolved to remove this source of uncertainty on the derived bias value of the Mg II absorption systems.

We now redo the fit to the measured  $\delta\tau_e(r_p, v)$  profiles presented in section 5, after replacing equation (16) by

$$\delta\tau_e(r_p, v) = \frac{b_{Mg} \tau_{e0}}{b_g \sqrt{2\pi}(1+q)} \frac{w_{gg}(r_p)H(z)}{(1+z)\sqrt{\sigma_0^2 + (xHr_p)^2}} \times \left[ e^{-(v-v_1)^2/2\sigma^2} + q e^{-(v-v_2)^2/2\sigma^2} \right]. \quad (25)$$

That is to say, we replace the power-law dependence of  $W_e$  on impact parameter by the model to the observed  $w_{gg}$  of Nuza et al. (2013). All the parameters except for  $b_{Mg}$  are kept fixed to the best fit obtained in section 5, and a new fit is obtained by matching only  $b_{Mg}$ . The function  $w_{gg}(r_p)$  is computed at our impact parameter bins by linear interpolation of the values of the model of Nuza et al. (2013). For convenience the fit is performed in the equivalent width space, namely,

$$W_e(r_p) = \tau_{e0} \frac{\lambda_{MgII}}{c} \frac{b_{Mg}}{b_g} \frac{w_{gg}(r_p)H(z)}{1+z} \quad (26)$$

The results we obtain for the Mg II absorption bias factor are

$$b_{Mg \text{ mean subtraction}} = 2.33 \pm 0.19, \quad (27)$$

$$b_{Mg \text{ variable smoothing}} = 1.14 \pm 0.36, \quad (28)$$

and the resulting fit for  $W_e(r_p)r_p$  are shown as the solid blue line for the mean subtraction method and the dashed red line

for the variable smoothing method in figure 10 (these lines are simply the rebinned thick solid black line shifted by the factor  $b_{Mg}/b_g$ ). The error on this bias factor includes only the uncertainty of the fit that assumes the bootstrap errors in our stacked spectra, and does not include the error of  $\tau_{e0}$ , assumed to be  $\tau_{e0} = 5.0 \times 10^{-4}$ . For completeness we also repeat the fit using Zhu et al. (2013) datapoints. The value we obtain is

$$b_{Mg \text{ ZHU13}} = 0.78 \pm 0.05, \quad (29)$$

Note that the error here is computed not from the bootstrap errors but directly from the  $\chi^2$  fitting instead. We neglect the fact that the datapoints are not independent.

We find a huge difference for  $b_{Mg}$  for the different methods. Thus, we stress once again the importance of the quasar continuum estimate. Getting the estimate right is crucial for the measurement of the bias and failing to do so may lead to really different results.

Our measurement for the mean subtraction method is discrepant from the previously reported values by Gauthier et al. (2009) of  $b_{Mg} = 1.36 \pm 0.38$ , and by Lundgren et al. (2009) of  $b_{Mg} = 1.10 \pm 0.24$ . Our result is closer to the bias factor measured for the galaxies, implying that most of the Mg II systems are associated to massive galaxies like the CMASS ones or even more massive. On the other hand, the measurement for the variable smoothing method is compatible with the previous ones. Finally the measurement using Zhu et al. (2013) datapoints is also not compatible with the reported values but for the opposite reason. It is too low.

However, as we discussed in section 5 and in the Appendix A, both the variable smoothing method and the method used in Zhu et al. (2013) underestimate the observed mean equivalent width. We have presented proof that it is indeed true for the variable smoothing case. We also argued that this is also likely to be true for the method used in Zhu et al. (2013). This means that the 'correct' value should be the  $2.33 \pm 0.19$  obtained for the mean subtraction method even though it is not compatible with the values reported in Gauthier et al. (2009) and Lundgren et al. (2009).

Note that our measurement of the bias factor remains subject to systematic uncertainties that will need to be improved: the determination of  $\tau_{e0}$ , the use of a wider velocity interval for determining the quasar continuum and the mean Mg II absorption compared to the ones used in this paper, and the use of a better modeling of the cross-correlation that includes redshift distortions in the regime of large impact parameters, and a more general density profile of Mg II absorbers in halos of different mass.

One possible reason for our high value of the Mg II bias is the degeneracy between  $\tau_{e0}$  and the Mg II bias. What we are actually fitting is the product of both. We can only recover the Mg II bias once we fix the value of  $\tau_{e0}$ . This means that an underestimation of  $\tau_{e0}$  will result in an overestimation of the Mg II bias. Thus, a more robust measurement of  $\tau_{e0}$  is required. Another possible reason for our high value of the Mg II bias is that the bias may decrease with the equivalent width of the Mg II absorbers, as found both by Lundgren et al. (2009) and Gauthier et al. (2009). Our method includes all the Mg II absorbers and measures their average bias, weighting each absorber by its equivalent width. This average bias would be larger than the one for strong, individually detected Mg II lines if the weak absorbers are asso-

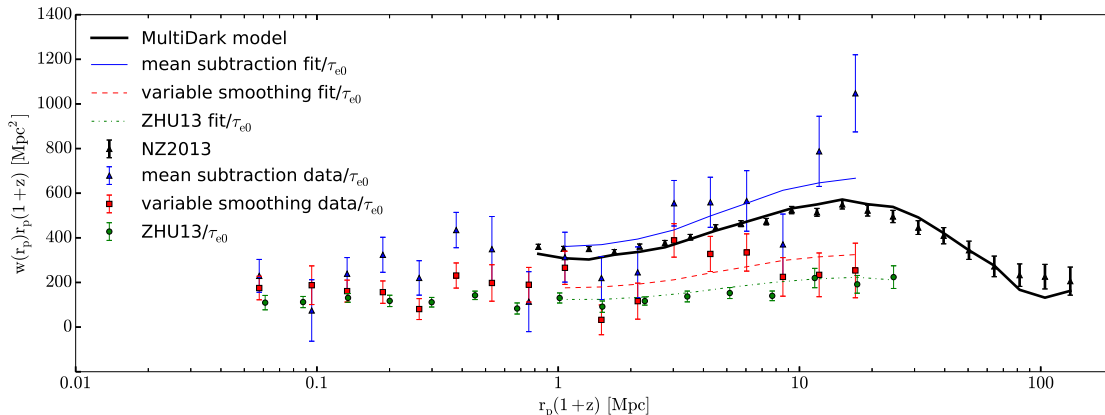


**Figure 10.** Projected correlation functions multiplied by the comoving impact parameter as a function of the comoving impact parameter  $r_p(1+z)$ . Thick black triangles with errorbars show the auto-correlation of CMASS galaxies from Nuza et al. (2013). Blue triangles, red squares and green circles are the mean equivalent width  $W_e(r_p)$  times the factor  $(1+z)/H(z)/\tau_{e0}$  (equal to the cross-correlation of Mg II systems and CMASS galaxies), times  $r_p(1+z)$  for the mean subtraction method, the variable smoothing method and measurements from Zhu et al. (2013) respectively. The thick solid black line is the MultiDark model prediction described in Nuza et al. (2013). The solid blue, the red dashed and the green dashed-dotted lines are the fit to  $W_e$  for the mean subtraction method, the variable smoothing method and measurements from Zhu et al. (2013) respectively. The ratio of the each of these lines with the thick solid black line is the ratio of bias factors,  $b_{\text{Mg}}/b_g$ .

ciated with massive halo environments, whereas absorbers of high equivalent width occur in galaxies hosted by low mass halos. Yet another possible explanation is our use of a limited velocity range for evaluating the projected cross-correlation of Mg II absorption and galaxies. We note that the high value of the bias we obtain is driven by the last point (at largest impact parameter) in figure 10. This point might be too high because linear redshift distortions have increased the density of Mg II absorbers in the interval used for integration, and decreased them in the interval used for continuum fitting. The projected cross-correlation should not be affected by these redshift distortions when it is computed by integrating over the whole line of sight, but at the largest impact parameters our integrating intervals are probably not large enough. This systematic effect can only be addressed by improving the continuum fitting method and the model of the cross-correlation in future work.

We now compare our results for the Mg II-galaxy cross-correlation with those of Zhu et al. (2013). The modeling of Zhu et al. (2013) involves a free parameter, which they designate as  $f_{\text{Mg II}}$ , that reflects the gas-to-mass ratio in halos (ignoring the degree of saturation of the absorption lines), and they assume a fixed density profile for the absorbers in halos. Zhu et al. (2013) do not relate this parameter to the mean absorption of the field population of Mg II absorbers, so they fit the amplitude of the cross-correlation with this unconstrained, free parameter. They determine a characteristic host halo mass for the Mg II absorbers of  $M_h \simeq 10^{13.5} M_\odot$  based on the presence of a feature in the shape of the cross-correlation at  $r_p \sim 1$  Mpc that reflects a transition from the 1-halo term to the 2-halo term in their modeling. The weakness of this feature implies a poor determination of this characteristic halo mass (see the contours in their figure 6, showing the large degeneracy with the  $f_{\text{Mg II}}$  parameter). Their determination of this halo mass is therefore highly dependent on their model of the halo density profile, and

does not generally match the total observed abundance of Mg II absorbers. Moreover, the Mg II absorbers are likely hosted in halos with a very broad mass range, which should cause a smoothing of any feature due to the transition from the 1-halo to the 2-halo term. The specific density profile of absorbers they assume has not been tested and is not theoretically well motivated. Mg II absorbers can be distributed in halos differently from galaxies, depending on the physics of gas cooling and galactic winds in halos. Auto-correlations and cross-correlations of galaxies of different types have been found to have widely different shapes (see, e.g., figures 15 and 16 in Zehavi et al. 2011) which do not always possess the clear feature that is predicted for a tracer that follows the dark matter profile in halos of a specific mass. Therefore, we think there is insufficient evidence for the presence of any feature in the Mg II-galaxy cross-correlation that may be used to determine a characteristic host halo mass.

Instead, we propose that the *amplitude* of this cross-correlation should be related to the field population of Mg II absorbers (e.g., through the effective optical depth  $\tau_{e0}$  that we have introduced), and can then be used to determine the mean bias factor  $b_{\text{Mg II}}$ , which should be equal to the mean bias factor of the host halos of the absorbers (weighted by their rest-frame equivalent width), and is robustly defined even if the range of host halo masses is very broad.

#### 6.4 The ratio of Mg II -absorbing gas to the total mass

Measurements of the average Mg II absorption around galaxies can be compared with mass measurements averaged in the same way obtained from weak gravitational lensing. This comparison was done in Zhu et al. (2013) to obtain an estimate for the ratio of gas mass to total mass in the halos around the CMASS galaxies of the BOSS survey. We now



examine this question to point out a number of uncertainties in this derivation.

In general, the total column density of MgII in an individual absorber,  $N_{\text{Mg II}}$ , is related to its integrated optical depth according to

$$N_{\text{Mg II}} = \frac{m_e c^2}{\pi e^2} \frac{W_\tau}{f \lambda_{\text{Mg II}}^2} = 1.13 \times 10^{20} \frac{W_\tau}{f \lambda_{\text{Mg II}}^2} \text{ cm}^{-2}. \quad (30)$$

where  $e$  and  $m_e$  are the electric charge and mass of the electron, and  $f = 0.921$  is the total oscillator strength of the MgII doublet. The integrated optical depth is

$$W_\tau = \int d\lambda \tau(\lambda), \quad (31)$$

where the integration is performed over a wavelength range that includes the entire absorption profile. However, the only quantity that is observed is the equivalent width,

$$W = \int d\lambda \left[ 1 - e^{-\tau(\lambda)} \right]. \quad (32)$$

When the optical depth of the absorber is much less than unity over the whole wavelength range, the absorber is unsaturated and  $W_\tau \simeq W$ . Otherwise, the column density is not directly measurable simply from the equivalent width. We now define an average saturation level for the population of absorbers,  $\bar{S}$ , as

$$\bar{S} = \frac{\int dW (\partial^2 \mathcal{N} / \partial W \partial z) W_\tau}{\int dW (\partial^2 \mathcal{N} / \partial W \partial z) W}. \quad (33)$$

Defining also  $x_{\text{Mg II}}$  as the fraction of magnesium atoms in the absorbing gas that are in the MgII ionized species,  $g_{\text{Mg}}$  as the fraction of magnesium in the absorbers that is in the gas phase (as opposed to dust grains), and  $Z_{\text{Mg}}$  as the magnesium mass fraction compared to that of the Sun (we use a solar magnesium abundance by mass of  $7.0 \times 10^{-4}$ , and a magnesium mass  $m_{\text{Mg}} = 4.07 \times 10^{-23}$  g), we obtain that the total gas mass surface density in the MgII absorbers is

$$\Sigma_g(r_p) = 9.15 \times 10^{-7} \frac{\bar{S}}{x_{\text{Mg II}} g_{\text{Mg}} Z_{\text{Mg}}} \frac{W_e(r_p)}{\text{\AA}} \text{ g cm}^{-2}. \quad (34)$$

The total mass surface density around a CMASS galaxy in the BOSS sample has also been measured using weak gravitational lensing. We can therefore obtain the ratio of gas in MgII absorbers to the total mass by combining the two observational measurements. We use the recent measurement by Miyatake et al. (2013) based on weak lensing measurements in the CFHTLenS survey area. As an example, we compute the gas-to-mass ratio at a comoving projected radius of  $r_p(1+z) = 3$  Mpc. The differential surface density measured by Miyatake et al. (2013) at this radius is  $\Delta\Sigma = \bar{\Sigma} - \Sigma \simeq 2 M_\odot \text{ pc}^{-2}$  (see their figure 7). Near this radius,  $\Delta\Sigma(r_p)$  is falling with radius roughly as  $r_p^{-1}$ , so the mean surface density within  $r_p$  is  $\bar{\Sigma} \simeq 2\Sigma$ , and we can therefore use  $\Sigma \simeq \Delta\Sigma$ . At this same radius,  $W_e \simeq 0.03$ , and substituting this value in equation (34), it produces  $\Sigma_g / \Sigma \simeq 8 \times 10^{-5} \bar{S} / (x_{\text{Mg II}} g_{\text{Mg}} Z_{\text{Mg}})$ . Using the mean ratio of baryons to total matter in the universe of  $\Omega_b / \Omega_m = 0.17$ , the fraction of baryons in the MgII absorbing gas would be  $\Sigma_g / \Sigma_b \simeq 5 \times 10^{-4} \bar{S} / (x_{\text{Mg II}} g_{\text{Mg}} Z_{\text{Mg}})$ .

Therefore, the fraction of baryons in the MgII clouds can be a small one even if the mean metallicity is relatively low. However, the mean saturation parameter  $\bar{S}$  is likely

much larger than unity, so it is possible that the MgII absorbers account for an important fraction of the baryons in galactic halos, and for the accreting material that fuels the star formation rate. We note that any further comparison of the detailed radial profiles of  $W_e(r_p)$  and  $w_{gg}(r_p)$  cannot be reliably used to infer a profile of the gas-to-mass ratio, because  $Z_{\text{Mg}}$  is likely to vary with  $r_p$ , since the heavy elements must have originated from galactic winds, and the values of  $\bar{S}$ ,  $x_{\text{Mg II}}$  and  $g_{\text{Mg}}$  may also vary substantially with  $r_p$ . The mean value of the gas-to-mass ratio is still highly uncertain because of the unknown value of  $\bar{S} / (x_{\text{Mg II}} g_{\text{Mg}} Z_{\text{Mg}})$ .

## 7 SUMMARY AND CONCLUSIONS

In this paper we have used the MgII line to measure the cross-correlation of MgII absorption and galaxies in BOSS. The large size of the samples we use (SDSS DR7 quasar catalog as background sample and DR11 CMASS galaxy catalog as foreground sample) enables a statistical approach to detect MgII absorption that is too weak to be detected individually and would otherwise be missed. We present a method to estimate the quasar continuum designed for this type of measurements and compare our results with those obtained by a more typical continuum estimate. Our main results can be summarized as follows:

- The method to fit the quasar continuum is crucial to measure the mean MgII equivalent width as a function of impact parameter. Methods that use the observed flux in the spectral region near the MgII line wavelength at the galaxy redshift to determine the continuum suffer from a systematic bias, because the absorption from individually undetected systems inevitably lowers the continuum estimate and causes an underestimate of the mean absorption. The tests presented in the Appendix A show that our mean subtraction method does not suffer from any systematic effect to the extent that we are able to discern.
- We find that the cross-correlation of MgII absorption and CMASS galaxies follows the shape of the CMASS galaxies auto-correlation at large scales. We use the CMASS auto-correlation model from Nuza et al. (2013) and the measured galaxy bias factor to derive a bias factor of MgII absorbers of  $b_{\text{Mg}} = 2.33 \pm 0.19$ . This value is substantially larger than the previous measurements by Gauthier et al. (2009) and Lundgren et al. (2009). This discrepancy may be due to a real difference, because our measurement includes a contribution from weak MgII absorption systems which may be more strongly clustered than strong absorbers, and may also be affected by our imperfect determination of the projected cross-correlation at large impact parameters owing to our limited integrating range. More accurate measurements and better modeling will be necessary to clarify this question.

## ACKNOWLEDGMENTS

Funding for SDSS-III has been provided by the Alfred P. Sloan Foundation, the Participating Institutions, the National Science Foundation, and the U.S. Department of Energy Office of Science. The SDSS-III web site is

<http://www.sdss3.org/>. IP and JM have been supported in part by Spanish grants AYA2009-09745 and AYA2012-33938.

SDSS-III is managed by the Astrophysical Research Consortium for the Participating Institutions of the SDSS-III Collaboration including the University of Arizona, the Brazilian Participation Group, Brookhaven National Laboratory, University of Cambridge, Carnegie Mellon University, University of Florida, the French Participation Group, the German Participation Group, Harvard University, the Instituto de Astrofísica de Canarias, the Michigan State/Notre Dame/JINA Participation Group, Johns Hopkins University, Lawrence Berkeley National Laboratory, Max Planck Institute for Astrophysics, Max Planck Institute for Extraterrestrial Physics, New Mexico State University, New York University, Ohio State University, Pennsylvania State University, University of Portsmouth, Princeton University, the Spanish Participation Group, University of Tokyo, University of Utah, Vanderbilt University, University of Virginia, University of Washington, and Yale University.

## REFERENCES

- Abazajian, K. N., Adelman-McCarthy, J. K., Agüeros, M. A., et al. 2009, *ApJS*, 182, 543
- Ahn, C. P., Alexandroff, R., Allende Prieto, C., et al. 2012, *ApJS*, 203, 21
- . 2013, ArXiv e-prints, arXiv:1307.7735
- Bahcall, J. N. 1975, *ApJL*, 200, L1
- Bahcall, J. N., & Spitzer, Jr., L. 1969, *ApJL*, 156, L63
- Bergeron, J., & Boissé, P. 1991, *A&A*, 243, 344
- Bergeron, J., & Stasińska, G. 1986, *A&A*, 169, 1
- Bernet, M. L., Miniati, F., & Lilly, S. J. 2010, *ApJ*, 711, 380
- Bolton, A. S., Schlegel, D. J., Aubourg, É., et al. 2012, *AJ*, 144, 144
- Bordoloi, R., Lilly, S. J., Kacprzak, G. G., & Churchill, C. W. 2012, ArXiv e-prints, arXiv:1211.3774
- Bordoloi, R., Lilly, S. J., Knobel, C., et al. 2011, *ApJ*, 743, 10
- Bouché, N., Murphy, M. T., & Péroux, C. 2004, *MNRAS*, 354, L25
- Bouché, N., Murphy, M. T., Péroux, C., Csabai, I., & Wild, V. 2006, *MNRAS*, 371, 495
- Chen, H.-W., Helsby, J. E., Gauthier, J.-R., et al. 2010a, *ApJ*, 714, 1521
- Chen, H.-W., Wild, V., Tinker, J. L., et al. 2010b, *ApJL*, 724, L176
- Churchill, C. W., Mellon, R. R., Charlton, J. C., et al. 2000, *ApJ*, 543, 577
- Churchill, C. W., Rigby, J. R., Charlton, J. C., & Vogt, S. S. 1999, *ApJS*, 120, 51
- Cole, S., & Kaiser, N. 1989, *MNRAS*, 237, 1127
- Dawson, K. S., Schlegel, D. J., Ahn, C. P., et al. 2013, *AJ*, 145, 10
- Eisenstein, D. J., Weinberg, D. H., Agol, E., et al. 2011, *AJ*, 142, 72
- Gauthier, J.-R., Chen, H.-W., & Tinker, J. L. 2009, *ApJ*, 702, 50
- Gauthier, J.-R., Tinker, J., & Chen, H.-W. 2008, in *COSPAR Meeting*, Vol. 37, 37th COSPAR Scientific Assembly, 980
- Gunn, J. E., Carr, M., Rockosi, C., et al. 1998, *AJ*, 116, 3040
- Gunn, J. E., Siegmund, W. A., Mannery, E. J., et al. 2006, *AJ*, 131, 2332
- Guo, H., Zehavi, I., Zheng, Z., et al. 2013, *ApJ*, 767, 122
- Johnson, S. D., Chen, H.-W., Mulchaey, J. S., et al. 2014, *MNRAS*, 438, 3039
- Kacprzak, G. G., Churchill, C. W., Evans, J. L., Murphy, M. T., & Steidel, C. C. 2011, *MNRAS*, 416, 3118
- Kacprzak, G. G., Churchill, C. W., & Nielsen, N. M. 2012, *ApJL*, 760, L7
- Kaiser, N. 1987, *MNRAS*, 227, 1
- Lanzetta, K. M., & Bowen, D. 1990, *ApJ*, 357, 321
- Lee, K.-G., Bailey, S., Bartsch, L. E., et al. 2013, *AJ*, 145, 69
- Lundgren, B. F., Wake, D. A., Padmanabhan, N., Coil, A., & York, D. G. 2011, *MNRAS*, 417, 304
- Lundgren, B. F., Brunner, R. J., York, D. G., et al. 2009, *ApJ*, 698, 819
- Lundgren, B. F., Brammer, G., van Dokkum, P., et al. 2012, *ApJ*, 760, 49
- Maller, A. H., & Bullock, J. S. 2004, *MNRAS*, 355, 694
- Miyatake, H., More, S., Mandelbaum, R., et al. 2013, ArXiv e-prints, arXiv:1311.1480
- Mo, H. J., & Miralda-Escudé, J. 1996, *ApJ*, 469, 589
- Narayanan, A., Misawa, T., Charlton, J. C., & Kim, T.-S. 2007, *ApJ*, 660, 1093
- Nestor, D. B., Turnshek, D. A., & Rao, S. M. 2005, *ApJ*, 628, 637
- . 2006, *ApJ*, 643, 75
- Nuza, S. E., Sánchez, A. G., Prada, F., et al. 2013, *MNRAS*, 432, 743
- Palanque-Delabrouille, N., Yèche, C., Borde, A., et al. 2013, *A&A*, 559, A85
- Rao, S. M., Turnshek, D. A., & Nestor, D. B. 2006, *ApJ*, 636, 610
- Sargent, W. L. W., Young, P. J., Boksenberg, A., Carswell, R. F., & Whelan, J. A. J. 1979, *ApJ*, 230, 49
- Schneider, D. P., Richards, G. T., Hall, P. B., et al. 2010, *AJ*, 139, 2360
- Smee, S. A., Gunn, J. E., Uomoto, A., et al. 2013, *AJ*, 146, 32
- Spitzer, Jr., L. 1956, *ApJ*, 124, 20
- Steidel, C. C. 1995, in *QSO Absorption Lines*, ed. G. Meylan, 139
- Steidel, C. C., Dickinson, M., & Persson, S. E. 1994, *ApJL*, 437, L75
- Tinker, J. L., & Chen, H.-W. 2008, *ApJ*, 679, 1218
- Vanden Berk, D. E., Richards, G. T., Bauer, A., et al. 2001, *AJ*, 122, 549
- York, D. G., Adelman, J., Anderson, Jr., J. E., et al. 2000, *AJ*, 120, 1579
- York, D. G., Vanden Berk, D., Richards, G. T., et al. 2005, in *IAU Colloq. 199: Probing Galaxies through Quasar Absorption Lines*, ed. P. Williams, C.-G. Shu, & B. Menard, 58–64
- Zehavi, I., Zheng, Z., Weinberg, D. H., et al. 2011, *ApJ*, 736, 59
- Zheng, Z., Berlind, A. A., Weinberg, D. H., et al. 2005, *ApJ*, 633, 791

Zhu, G., & Ménard, B. 2013a, ApJ, 773, 16  
 —. 2013b, ApJ, 770, 130  
 Zhu, G., Ménard, B., Bizyaev, D., et al. 2013, ArXiv e-prints, arXiv:1309.7660

**APPENDIX A: TESTS OF THE CONTINUUM FITTING METHODS**

The method to fit the quasar continuum is a crucial part of the measurement of the mean MgII absorption equivalent width as a function of impact parameter from a galaxy,  $W_\tau(b)$ , presented in this paper. The two methods we have used produce a different result, which is also different from the result reported by Zhu et al. (2013). It is therefore important to perform tests on these methods that can reveal the presence of systematic errors in the  $W_\tau(b)$  estimates. This appendix presents the results of three tests. The first one (section A1) checks for any systematic mean absorption that might be artificially introduced by the continuum fitting method when there is no correlation between MgII absorbers and galaxies. The second one (section A2) verifies that the correct equivalent width of an individually detected MgII absorption system in a spectrum is correctly recovered. Finally, section A3 reveals the effect on the fitted continuum of the presence of weak absorbers that are individually undetected, and the way these absorbers can bias the estimate of the mean equivalent width.

**A1 Systematic errors in the absence of correlations**

One might suspect that a small average absorption (either positive or negative) is artificially introduced by the method to fit the continuum, even when the regions selected to search for absorbers are completely random and should therefore have no average absorption. This might happen if the quasar continuum is systematically overestimated or underestimated, depending in a complex manner on the varying noise properties and the shape of the true quasar continuum. To test for this possibility, we have remeasured the mean MgII equivalent widths after rotating the right ascension coordinate of all the quasar by 5 and 10 degrees, in the two possible directions, and after increasing and decreasing the redshift of the galaxies by 0.05. These separations are large enough to make any residual cross-correlation of galaxies and MgII absorbers completely negligible, so the measured correlation should be consistent with zero. Note that this procedure ensures that the auto-correlations that are present among the MgII absorbers, quasars and galaxies are preserved, so their contribution to the measurement errors of the cross-correlation is the same.

The result of this test is shown in figure A1, in the left panel for the mean subtraction method and the right panel for the variable smoothing method. The real data set is shown as big red circles with errorbars, after dividing by the best-fit power-law model that is described in Section 4 and plotted in figure 8. The average of 6 mock data sets are shown also after dividing by the same model as blue stars. In the absence of any systematics, the mean absorption in the mock data sets is expected to be zero, whereas

the real data should produce a ratio to the best-fit model that is consistent with one. The results do not show any systematic errors for the mean subtraction method. There appears to be a small negative systematic absorption that is introduced by the variable smoothing method, as indicated by the negative values of the mock sample in the right panel, at large impact parameters (where the mean equivalent width can be measured with the smallest errorbar). This average negative absorption is approximately equal to the best-fit model prediction at  $\sim 10$  Mpc, or  $\sim 0.3 \text{ km s}^{-1}$  (see figure 8). This result may be due to some subtle effect in the variable smoothing method that introduces a small bias by systematically underestimating the continuum in the absence of real absorption lines, possibly due to occasional false identifications of noise spikes as real absorbers. As we shall see below, the variable smoothing method is actually affected by a more serious systematic error that partially eliminates the contribution of weak absorption systems to the mean equivalent width.

**A2 Tests of the equivalent width measurement for individually detected systems**

We now test that the mean equivalent width measured for absorbing systems that are individually clearly detected above the noise agrees with other well established methods. For this purpose, we use the MgII absorber catalogue of Zhu & Ménard (2013b), which contains 35,752 absorption systems from the SDSS DR7 quasar spectra sample. The integrated equivalent widths we obtain for systems in this catalogue, using our two methods of mean subtraction and variable smoothing, are compared with the equivalent widths provided in the catalogue in figure A2. There is a large scatter in the equivalent widths obtained with different methods. This result is not surprising, because the noise can change the determination of the continuum in random ways in different methods. In particular, in the method of the mean subtraction, the equivalent width is obtained by integrating the absorbed fraction over a wide interval around the absorber, according to equation (18), adding noise to the estimate. However, the average of the equivalent width estimator in our mean subtraction method, shown by the black points in figure A2 (with an rms dispersion indicated by the errorbars), agrees very well with the equivalent width provided by the Zhu & Ménard (2013b) catalogue. The variable smoothing method apparently suffers from a bias causing a 10 to 20% increase of the average of the equivalent width (see black points in middle panel of figure A2), which may be due to a tendency of this method to overestimate the continuum level around detected absorption lines.

**A3 Impact of individually undetected systems on the mean equivalent width**

We now test how the presence of weak absorption systems that cannot be individually detected in a single spectrum but contribute to the mean equivalent width as a function of impact parameter from a galaxy can bias the estimate of the quasar continuum in the different methods we use. For this purpose, artificial absorbers are introduced in a spectrum, and then we refit the continuum and measure the change in the measured equivalent width.

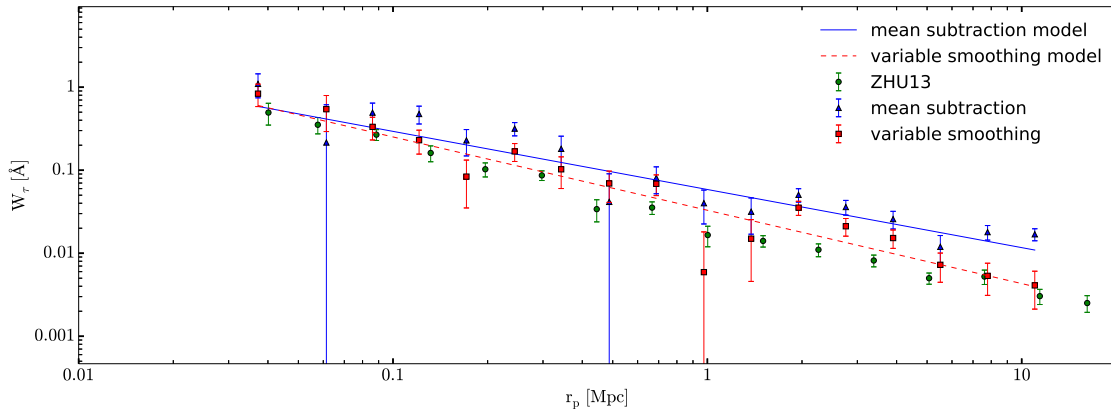


**Figure A1.** Ratio of the mean equivalent width in stacked spectra to the best-fit power-law model prediction, for the real data sample (big red circles), and for the average of 6 mock samples (blue stars). Errorbars are computed with the bootstrap method. This ratio should be consistent with zero for the mock sample in the absence of systematic errors, and with unity for the real data if the power-law model provides a good fit to the data.

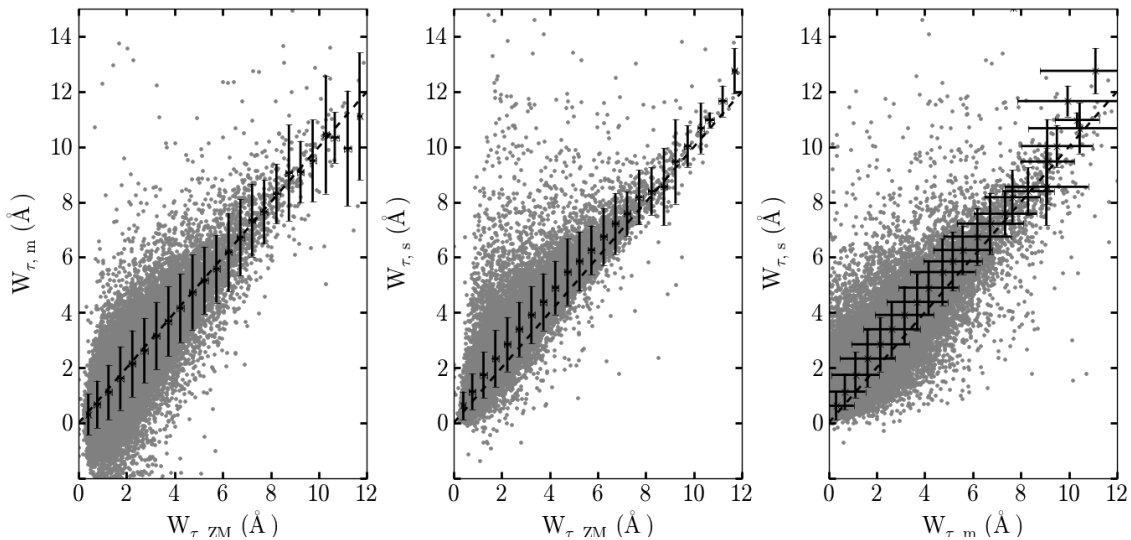


**Figure A2.** Comparison of the equivalent width estimates from different methods (see Section 3). From left to right, equivalent widths measured using the mean subtraction method,  $W_m$ , versus the value of the Zhu & Menard catalogue,  $W_{ZM}$ ; variable smoothing method value,  $W_s$ , versus  $W_{ZM}$ ; and  $W_s$  versus  $W_m$ . Black points are the average values in bins of  $\Delta W = 0.5$  in the horizontal axis, with the dispersion in each bin indicated by the errorbars. One-to-one correspondence is marked by the black dashed line for visual guidance.

As an illustrative example, we have selected a set of 10 random quasar spectra, and we have introduced absorbers at 10 random redshift values and computed the average values for the recovered width. The absorbers are inserted with a double Gaussian profile in the optical depth, as expected for the Mg II doublet,

$$\tau(v) = \frac{W_0}{\sqrt{2\pi}\sigma} \left( \frac{2}{3} \exp[-(v-v_1)^2/2\sigma^2] + \frac{1}{3} \exp[-(v-v_2)^2/2\sigma^2] \right), \quad (\text{A1})$$

where  $W_0$  is the total equivalent width of the doublet and  $\sigma$  is velocity dispersion. The zero velocity is convention-

ally chosen to be the central position of the Mg II line for an unsaturated line, so that  $v_1 = -256.05 \text{ km s}^{-1}$  and  $v_2 = 513.28 \text{ km s}^{-1}$ . In the absence of any inserted absorber, the continuum determined in this spectrum is  $c(v)$ , the flux is  $f(v)$ , and the transmitted fraction is  $F(v) = f(v)/c(v)$ . This results in a certain value of the integrated equivalent width  $W$  measured over the interval  $-2000 \text{ km s}^{-1} < v < 2000 \text{ km s}^{-1}$ , by integrating  $F(v)$  over this range. To insert the absorber, the spectral flux is modified according to

$$f'(v) = f(v) - c(v)(1 - \exp[-\tau(v)]) . \quad (\text{A2})$$

Then, a new continuum  $c'(v)$  is determined with the new flux, and a new transmitted fraction  $F'(v) = f'(v)/c'(v)$  is

derived. Finally, the new equivalent width  $W'$  is determined by integrating  $F'$  over the same velocity interval.

The change in equivalent width caused by the insertion of an absorber,  $\Delta W = W' - W$ , is plotted in figure A3 as a function of the equivalent width  $W_i$  of the inserted absorber, obtained by integrating  $1 - \exp[-\tau(v)]$  over the same velocity interval that is used for determining  $W$  and  $W'$  ( $W_i$  is nearly equal to  $W_0$  in equation A1, except that the integrating interval does not extend to infinity). The different lines correspond to different values of the absorber velocity dispersion,  $\sigma$ . The solid blue lines represent the mean subtraction method, and they coincide precisely with  $\Delta W = W_i$  for all values of  $\sigma$ . The result, as expected, is that the continuum determined by this method is unaffected by the presence of the absorbers that have narrow widths compared to the chosen integrating interval width of  $4000 \text{ km s}^{-1}$ . The reason is that, in the mean subtraction method, the continuum  $c'(v)$  is determined using only the measured flux outside of this interval.

On the other hand, the variable smoothing method (dashed red lines in figure A3) is strongly biased to lowering the estimated continuum in response to the presence of a weak absorption system. The result is that the change caused by the absorber in the estimated equivalent width,  $\Delta W$ , can be much less than the true value, and the difference is a complex function of the equivalent width  $W_0$ , the velocity dispersion and the signal-to-noise ratio of the spectrum. The underestimate of the continuum level is naturally smaller for narrower lines (lower  $\sigma$ ), because the lines are detected and eliminated from the continuum estimation for lower values of  $W_0$ .

To summarize, the three tests of our continuum fitting methods presented in this Appendix demonstrate that the variable smoothing method suffers from several systematic errors. The first test shows that a small negative absorption, of equivalent width  $\sim -0.3 \text{ km s}^{-1}$ , is induced where there is none. The second test indicates that the equivalent width of strong, detected systems is overestimated by 10 – 20%. Finally, the third test shows that for weak systems, the continuum is systematically underestimated, thereby strongly reducing the contribution of these systems to the measured equivalent width. However, the mean subtraction method successfully passes all these tests and should therefore provide a reliable estimate of the stacked equivalent width as a function of impact parameter.

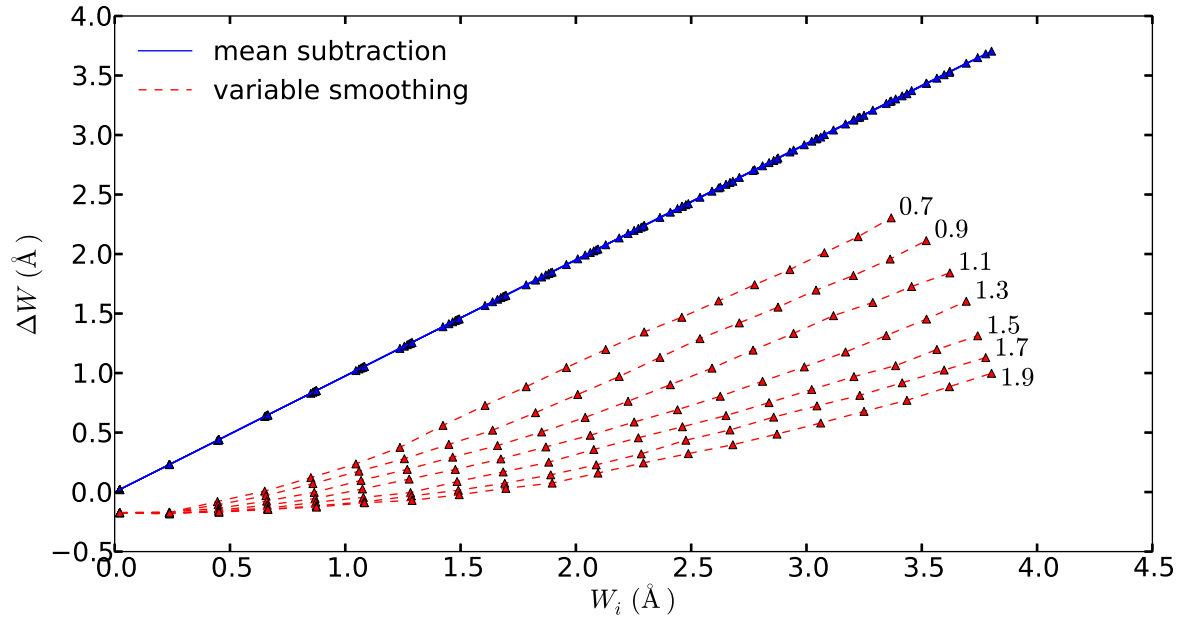


**Figure A3.** Change in the measured equivalent width,  $\Delta W$ , caused by the insertion of an absorbing system with equivalent width  $W_i$ , for the mean subtraction method (solid blue lines) and the variable smoothing method (dashed red lines). Results are shown as a function of the velocity dispersion  $\sigma$ , with values indicated to the right of the lines in  $\text{\AA}$ . The blue lines all nearly coincide at  $\Delta W = W_i$ . Points show the values of  $W_i$  for which  $\Delta W$  has been computed; the sudden changes in the red lines indicate discontinuities in the variable smoothing method as the inserted line becomes detected or covers different pixels, which causes a change in the continuum estimate.